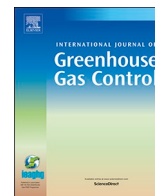




ELSEVIER

Contents lists available at ScienceDirect

## International Journal of Greenhouse Gas Control

journal homepage: [www.elsevier.com/locate/ijggc](http://www.elsevier.com/locate/ijggc)Application of natural and artificial tracers to constrain CO<sub>2</sub> leakage and degassing in the K-COSEM site, South KoreaYeoJin Ju<sup>a</sup>, Stan E. Beaubien<sup>b</sup>, Seong-Sun Lee<sup>a</sup>, Dugin Kaown<sup>a</sup>, Doshik Hahm<sup>c,d</sup>, Sanghoon Lee<sup>a</sup>, In-Woo Park<sup>a</sup>, Keyhong Park<sup>d</sup>, Seong-Taek Yun<sup>e</sup>, Kang-Kun Lee<sup>a,\*</sup><sup>a</sup> School of Earth and Environmental Sciences, Seoul National University, 1 Gwanak-ro, Gwanak-gu, Seoul, 08826, South Korea<sup>b</sup> Dipartimento di Scienze della Terra, Università di Roma "La Sapienza", Piazzale Aldo Moro 5, 00185, Roma, Italy<sup>c</sup> Department of Oceanography, Pusan National University, Busan, South Korea<sup>d</sup> Division of Polar Ocean Science, Korea Polar Research Institute, Incheon, South Korea<sup>e</sup> Department of Earth and Environmental Sciences and the Environmental Research Laboratory (EGRL), Korea University, Seoul, 136-701, South Korea

## ARTICLE INFO

## Keywords:

Carbon capture and storage  
Geological storage  
CO<sub>2</sub> leakage  
Noble gas tracing  
Artificial tracer  
Geochemical tracing

## ABSTRACT

Although Carbon Capture and Storage (CCS) has been demonstrated successfully on many occasions, the potential leakage of deep sequestered CO<sub>2</sub> into shallow groundwater remains a concern. To address this, an artificial injection experiment was performed at the K-COSEM test site in Eumseong, South Korea, that involved the release of CO<sub>2</sub>-infused water (16.9 kg of CO<sub>2</sub> in 5 m<sup>3</sup>) containing He and Kr tracers into a shallow, heterogeneous, weathered-granite aquifer. The initial CO<sub>2</sub>-fluid was slightly oversaturated at the subsurface injection point, and thus the plume was expected to initially degas CO<sub>2</sub> before equilibrating at *in-situ* conditions. Monitoring of carbonate system parameters in nearby observation wells helped define the evolution of the injected fluids, while the noble gas tracers were used to clearly define the physical behavior of the CO<sub>2</sub> plume (including an estimate of degassed CO<sub>2</sub> equal to 0.9–3.1%). This study demonstrates the potential use of noble gases for monitoring CO<sub>2</sub> leakage in shallow aquifers, constraining mass balance and phase changes of leaking fluids, and better understanding local flow pathways. Furthermore, breakthrough of noble gases in this study was different from some previous experiments, suggesting that monitoring efficiency of these tracers may depend on leakage and site conditions.

## 1. Introduction

Carbon Capture and Storage (CCS) is a climate change mitigation technology that involves isolating large volumes of man-made CO<sub>2</sub> in the deep subsurface instead of releasing it to the atmosphere (IPCC, 2005). Although CCS has been demonstrated successfully on many occasions (Celia, 2017), the potential for CO<sub>2</sub> leakage and its possible impact on shallow groundwater resources remains a concern (Boyd, 2016). To address this, research has been conducted to better understand the various chemical and physical processes during fluid migration, the potential impacts on groundwater quality, and to develop groundwater monitoring tools. This has been done using both controlled CO<sub>2</sub>-injection experiments in shallow aquifers (Lee et al., 2016, and references therein) and natural sites of CO<sub>2</sub> leakage to the surface (e.g., Keating et al., 2010; Beaubien et al., 2014).

In this regard, various geochemical parameters have been shown to be effective tools (Yang et al., 2014; Lee et al., 2016). For example, the monitoring of CO<sub>2</sub> itself, as well as its δ<sup>13</sup>C signature, is a fundamental starting point to uncover the origins of CO<sub>2</sub> anomalies in groundwater systems (Ballentine et al., 2001; Sherwood Lollar et al., 1997). However, the complex interaction of this gas in various chemical and biological reactions has led to the study of other, more conservative tracers (Risk et al., 2015; Kharaka et al., 2006; Shevalier et al., 2013). For example, Risk et al. (2015) evaluated the detectability of multiple tracers using a signal to noise ratio (SNR) approach, showing that inert tracers like noble gases were superior to CO<sub>2</sub> concentration measurements due to their limited natural variability in groundwater systems. In shallow settings this baseline is primarily controlled by exchange with atmospheric gases in the vadose zone (Xe, Kr, Ar, Ne), whereas in deeper reservoirs, radiogenic <sup>4</sup>He and <sup>40</sup>Ar, fissionogenic Xe,

\* Corresponding author.

E-mail addresses: [jinee18@snu.ac.kr](mailto:jinee18@snu.ac.kr) (Y. Ju), [stanley.beaubien@uniroma1.it](mailto:stanley.beaubien@uniroma1.it) (S.E. Beaubien), [soon3311@snu.ac.kr](mailto:soon3311@snu.ac.kr) (S.-S. Lee), [dugin1@snu.ac.kr](mailto:dugin1@snu.ac.kr) (D. Kaown), [hahm@pusan.ac.kr](mailto:hahm@pusan.ac.kr) (D. Hahm), [lshlsh2311@snu.ac.kr](mailto:lshlsh2311@snu.ac.kr) (S. Lee), [inwoo0415@snu.ac.kr](mailto:inwoo0415@snu.ac.kr) (I.-W. Park), [inwoo0415@snu.ac.kr](mailto:inwoo0415@snu.ac.kr) (K. Park), [styun@korea.ac.kr](mailto:styun@korea.ac.kr) (S.-T. Yun), [jinee18@snu.ac.kr](mailto:jinee18@snu.ac.kr) (K.-K. Lee).<https://doi.org/10.1016/j.ijggc.2019.05.002>

Received 15 October 2018; Received in revised form 2 May 2019; Accepted 2 May 2019

Available online 14 May 2019

1750-5836/ © 2019 Elsevier Ltd. All rights reserved.

nucleogenic He and Ne, mantle  $^{129}\text{Xe}$ , and primordial  $^3\text{He}$  are all possible noble gas sources (Holland and Gilfillan, 2013). While noble gases are chemically and biologically inert, each species has its own physical characteristics (solubility, molecular size, diffusion coefficient) which influence its subsurface behavior (e.g., Kilgallon et al., 2018). Understanding and exploiting these differences means that noble gases can be powerful tracers to better understand physical processes related to  $\text{CO}_2$  source identification, fluid flow and phase partitioning.

For example, noble gas distributions have been used to determine the origin of  $\text{CO}_2$  in deep reservoirs (Gilfillan et al., 2008), to fingerprint gases from different lithological units (Györe et al., 2018), and to identify the leakage of deep-origin  $\text{CO}_2$  into shallow aquifers (Gilfillan et al., 2011; Lafortune et al., 2009; Wilkinson et al., 2010). Recently, Gilfillan et al. (2017) illustrated the potential of this approach in a real-world setting by using noble gases to show that near-surface  $\text{CO}_2$  anomalies observed above the Weyburn-Midale  $\text{CO}_2$ -EOR site in western Canada were due to shallow biological processes and not caused by leakage from the underlying  $\text{CO}_2$  injection reservoir.

Injection of noble gas tracers together with  $\text{CO}_2$  has also been performed in several injection experiments in deep reservoirs to understand flow dynamics, to distinguish between artificially injected and naturally occurring  $\text{CO}_2$ , and to develop possible early warning tools (Lu et al., 2012; Nimz and Hudson, 2005; Stalker et al., 2009, 2015). A conceptual model explaining some of the trends observed in such field tests is provided by Kilgallon et al. (2018), based on laboratory-scale, gas-phase column experiments. This work illustrates how the noble gases migrate with the bulk  $\text{CO}_2$ , but at different velocities as a function of the physical properties of the individual gases. For example, these authors show that He had the slowest noble gas arrival time (perhaps counterintuitively) due to diversion of this smaller molecule into disconnected and dead-end pores, and that all noble gases migrated much faster than the co-injected  $\text{CO}_2$  but that Kr and Xe provided the most robust early warning signal.

These different physical characteristics have also been exploited to better understand phase partitioning and the physical interaction of  $\text{CO}_2$  or  $\text{CH}_4$  with deep groundwater (Darrah et al., 2014; Gilfillan et al., 2008; Sathaye et al., 2014). For example, LaForce et al. (2014) conducted field tests at the CO2CRC Otway site and performed associated 1D simulations to quantify residually trapped  $\text{CO}_2$ , finding that estimates based on both Kr and Xe data were the same within the accuracy of the method. Temporal sampling of the Cranfield enhanced oil recovery (EOR) field has shown how non-radiogenic noble gas isotopes in the formation water were stripped by the injected  $\text{CO}_2$  and that only about 0.2% of the injected  $\text{CO}_2$  occurs in the dissolved phase (Györe et al., 2015, 2017). This was done by focusing on gas ratio changes of noble gases, as the species are preferentially partitioned into the free  $\text{CO}_2$  bubbles and the speed of phase-transition is proportional to the elemental mass (Ballentine et al., 2002). This phase partitioning process retards the arrival time of noble gases at monitoring wells, with the extent of retardation appearing to be related to the solubility of each noble gas component (Zhang et al., 2011).

Although noble gases have been applied extensively in the deep CCS injection experiments described above, to our knowledge they have not been used much in the various shallow aquifer  $\text{CO}_2$  injection tests that have been conducted to study the possible impact of leakage on potable water supplies or to test near-surface monitoring techniques. These experiments, often performed at less than 20 m depth, have mainly consisted of the injection of gaseous  $\text{CO}_2$  into unconsolidated sediments (e.g., Cahill et al., 2014; Humez et al., 2014; Schulz et al., 2012; Peter et al., 2012) or, in one case, fractured igneous rock (Susanto et al., 2016). In contrast, Trautz et al. (2012) injected dissolved  $\text{CO}_2$  in shallow sediments after conducting a separate, short-term tracer test using dissolved Ar.

The present work describes a shallow groundwater injection experiment conducted at the Korea  $\text{CO}_2$  Storage Environmental Management Research Center (K-COSEM) test site near Eumseong,

South Korea, a unique facility defined by its weathered soils and associated heterogeneous flow field that presents challenges for  $\text{CO}_2$  plume monitoring (Lee et al., 2017a, 2017b). This experiment involved injecting groundwater infused with  $\text{CO}_2$  and noble gases (He, Kr and Ar) to mimic a minor  $\text{CO}_2$  leakage event (16.9 kg) in a shallow aquifer system, followed by geochemical monitoring using a number of closely spaced observation wells. The complex hydrogeology of the site and the innovative application of noble gas tracers in this shallow injection experiment allowed us to focus on two main objectives. First, to evaluate the monitoring ability of noble gas tracers associated with  $\text{CO}_2$  leakage and to compare their behavior with various other parameters (e.g., carbonate system species, temperature, electrical conductivity, etc.), focusing on local flow-related issues like migration pathways, mixing between injected and *in-situ* groundwaters, and the potential use of noble gases as an early warning monitoring tool. Second, to use the noble gas data to estimate the amount of  $\text{CO}_2$  that degassed during the experiment and to constrain the  $\text{CO}_2$  mass balance based on gas-water phase partitioning.

## 2. Site description

The K-COSEM test site was constructed in 2014 to study shallow-depth subsurface and surface environmental impacts caused by the controlled injection of  $\text{CO}_2$  (Lee et al., 2017b). It is located on private land in the Upper Miho River watershed in Eumseong county, South Korea (Fig. 1a), and is surrounded by slightly hilly agricultural lands. The geology of the area mainly consists of Precambrian gneiss, Jurassic Daebo granite, and Cretaceous intrusive igneous rocks that are covered by Quaternary alluvium in unconformity. Based on borehole data, the site includes weathered soils consisting of medium to coarse grained silty sand (0–30 m), weathered biotite granite (30–70 m), and unweathered biotite granite bedrock (> 70 m) (Ju et al., 2018).

A total of 24 monitoring wells have been drilled at the K-COSEM site, 10 of which were used for the injection experiment in this study (Figs. 1 and 2). The five borehole series wells (BH) were sampled for baseline noble gas measurements while the other five wells were used to monitor plume migration during the experiment. These monitoring wells include the partially screened well (PS-04), the injection well (IW), the borehole screened well (BS-09) and the two saturated zone monitoring wells (SMW1 and SMW2) (Figs. 1,2); see Lee et al., 2017b for more details.

The piezometric surface is located at a depth of about 17 m. Regional groundwater flow is to the SE (Fig. 1) however localized flow is more complicated, as verified by multiple inter-well pumping tests (Lee et al., 2017b). Hydraulic conductivity values range from 4.0E-06 m/s to 2.0E-05 m/s based on push-and-pull tracer tests conducted using  $\text{Cl}^-$  and  $\text{SF}_6$  tracers, with variations due to the heterogeneous distribution of weathered materials (Kim et al., 2018). Lee et al. (2017a) also observed these heterogeneous permeability distributions in electrical resistivity survey results, which were then used in numerical simulations that showed fast initial movement of the plume along a high permeability zone near the injection well.

## 3. Materials and methods

### 3.1. Injection of $\text{CO}_2$ with artificial tracers

The experiment involved injection of 5 m<sup>3</sup> of  $\text{CO}_2$ -infused groundwater (i.e. 16.9 kg of  $\text{CO}_2$ ) followed by 2.5 m<sup>3</sup> of chaser fluid (see description below) into a shallow groundwater system at a rate of 16.34 L/min over a period of 459 min (from 17:00 on 29/11/2016 to 00:40 on 30/11/2016) using a submersible and controllable quantitative pump (model MP1, Grundfos). A schematic drawing of the injection infrastructure is shown in Fig. 3. Injection was performed at 21–24 m below ground surface (about 4.5–7.5 m below the water table) in an interval isolated with a packer. The ambient surface weather

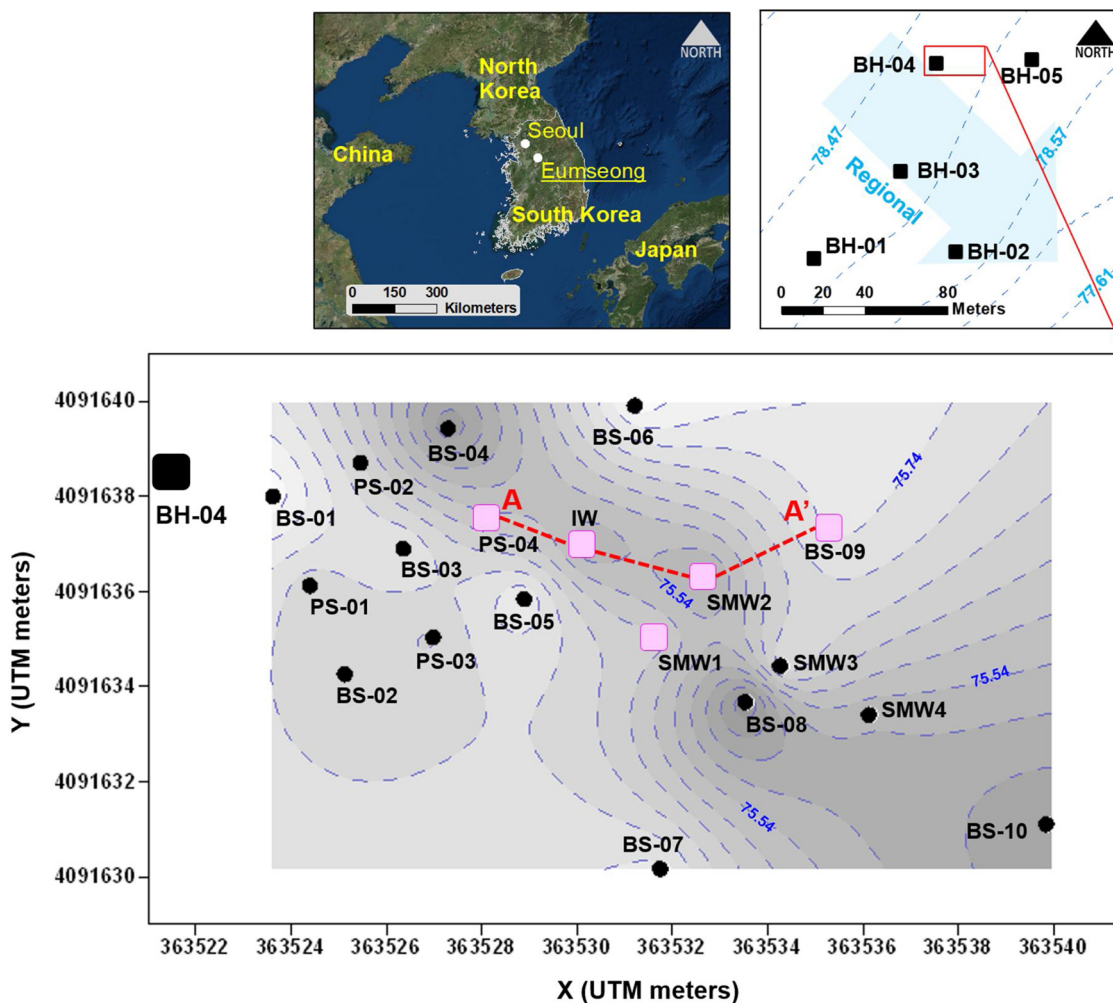


Fig. 1. Geographical location of K-COSEM study site. Top left - location of the K-COSEM study site. Top right – location of five BHs - boreholes (black squares) with the regional piezometric surface (dashed blue lines) and groundwater flow direction (blue arrow) (from Ju et al., 2018). Bottom - the piezometric surface (dashed blue lines) measured in the study site wells (PS - partially screened; IW - injection well; BS - borehole screened; and SMW - saturated zone monitoring wells). The pink squares show the five wells that were monitored during the experiment while the dashed red line A-A' shows the trace of the profile in Fig. 2.

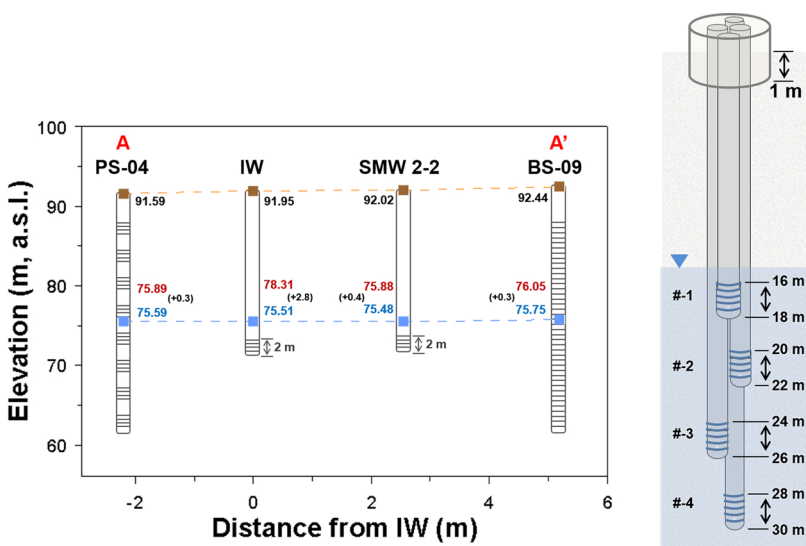


Fig. 2. Schematic drawings illustrating well design, layout, and water table response. The drawing on the left shows relative locations of the main wells discussed in the text and shown in Fig. 1; a.s.l. = above sea level. Screened intervals are represented as horizontal black lines in the different types of wells. Pre-injection groundwater levels are given in blue text and subsequent mounding during injection is given in red text (differentials reported in brackets). The drawing on the right shows the design of the multi-level Saturated zone Monitoring Wells (SMW); b.g.s. = below ground surface.

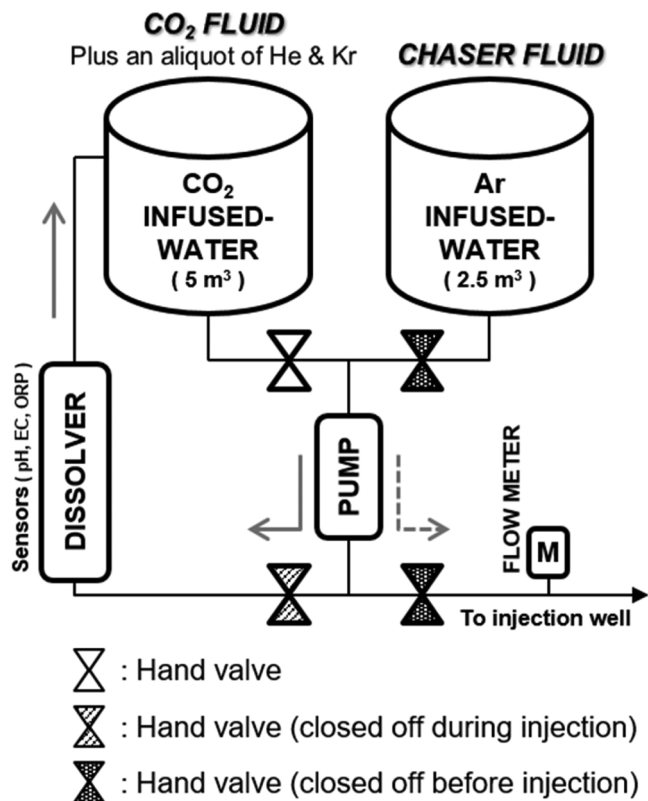


Fig. 3. Injection system for making the two gas-infused groundwater solutions.

conditions during injection were predominantly sub-zero with the absence of precipitation.

The CO<sub>2</sub>-saturated solution was made by continuously bubbling pure CO<sub>2</sub> gas into groundwater pumped from the test site inside a holding tank on the surface. The tank was not sealed and thus the system was equilibrated with pure CO<sub>2</sub> at approximately 1 atm. A total of 20.2 cm<sup>3</sup> STP of Kr and 15.6 cm<sup>3</sup> STP of He were then added to the CO<sub>2</sub>-charged solution prior to its injection into the groundwater system.

As in other studies (e.g. Hebig et al., 2015), a chaser fluid was then used to push the initially injected fluid into the surrounding permeable rock to minimize the hydraulic effect of the borehole and its surrounding gravel pack on breakthrough results. Although chaser fluids typically consist of unaltered groundwater, in this case it was saturated with Ar to obtain concentrations higher than those created for He and Kr in the CO<sub>2</sub>-infused fluid. This elevated Ar concentration was created to help distinguish this artificial tracer from the natural background levels (e.g., Trautz et al., 2012).

### 3.2. Sampling

Baseline water samples were collected prior to the injection test to assess natural variability. This consisted of a single noble gas sampling campaign (March 6, 2015 to March 7, 2015), a single TIC sampling campaign just before injection (November 28, 2016) and eight water quality sampling campaigns (February 24, 2016 to November 21, 2016). Water sampling for the injection experiment was performed 12 times within 4 months (114 days) following the termination of injection.

Water was collected using a submersible and controllable quantitative pump (model MP1, Grundfos). In the various observation wells, the well volume was purged three times prior to sampling. In contrast, the injection well was sampled from above the packer during the first two days (to maintain isolation of the injected fluids) without purging; after the second day the packer was removed and the well was purged

three times before sampling.

Water samples for noble gas analysis were collected in atmospherically isolated copper tubes (28 mL) and sealed with stainless steel clamps. TIC samples were immediately treated with HgCl<sub>2</sub> to prevent biological activity and then stored in sealed borosilicate bottles until analysis (Dickson et al., 2007). Samples to measure the CO<sub>2</sub> concentration (C<sub>0</sub>) in the first injected fluid were collected by filtering 90 mL of water through 0.02 μm syringe filters in a closed system and storing them in serum vials containing 10 mL of 1 M NaOH solution. All water samples were stored at a low temperature (under 4°C) using an ice box or refrigerator.

### 3.3. On-site measurements

Real-time, *in-situ* monitoring of water level, temperature and electrical conductivity was performed at 10 min intervals using the LTC Levellogger Junior (Solinst) for 5 months before and over the course of the experiment. These units were installed in the five BH wells, and in PS-04, IW, BS-09, SMW-1, and SMW-2 (Fig. 1). Salinity and pH were measured *in-situ* periodically using a YSI portable system (YSI Inc./Xylem Inc., USA) and alkalinity was determined by acid titration with 0.05 M HNO<sub>3</sub> in the field.

### 3.4. Laboratory analyses

The noble gas samples obtained prior to CO<sub>2</sub> injection (BH series) were analyzed at the University of Utah (Aeschbach-Hertig and Solomon, 2013; Solomon et al., 2015). Gases were first extracted from a groundwater sample and stored in a stainless steel flask (Bayer et al., 1989). Excessive water vapor and other condensable gases were then removed using cryogenic traps (Lott, 2001) and SAES getters. All species except He were quantified using a quadrupole mass spectrometer (Stanford Research Systems RGA300) while He was quantified using a sector-field mass spectrometer (Mass Analyser Products model MAP 215-50). The measured responses of He, Ne, Ar, Kr and Xe were converted to air quantity by calibrating them with dry atmospheric air. The reproducibility of this method was within 1% for He and within 5% for the other noble gases (Manning et al., 2005; Solomon et al., 2010).

Instead, the noble gas samples obtained following CO<sub>2</sub> injection were analyzed at the Korea Polar Research Institute (KOPRI) using an automated system (Kim et al., 2016) similar to that of Stanley et al. (2009). Gases were extracted from the groundwater samples under high vacuum (~10<sup>-7</sup> mbar) and stored in aluminosilicate glass ampoules (Lott and Jenkins, 1998). Before injecting samples into a quadrupole mass spectrometer (Stanford Research Systems RGA200), excessive water vapor and other condensable gases were removed in a purification line equipped with cryogenic traps and getters (hot and cold St 101, SAES). He, Ar, and Kr were calibrated against air standards of 0.9 and 2.7 mL STP, covering the wide concentration range of the injected tracers. The reproducibility for the post-injection data was within 5% for three gases.

Total dissolved inorganic carbon (TIC = [CO<sub>2</sub>] + [HCO<sub>3</sub><sup>-</sup>] + [CO<sub>3</sub><sup>2-</sup>]) analyses were performed at the Core Laboratory of Innovative Marine and Atmospheric Technology (CLIMATE), Pohang University of Science and Technology (POSTECH). TIC concentration was determined via coulometric titration, using the Versatile INstrument for the Determination of Total Alkalinity (VINDTA) system (Marianda, Kiel, Germany). The accuracy of the TIC measurement was vetted daily against reference materials with known TIC values (certified by A. Dickson, Scripps Institution of Oceanography, San Diego, USA). The measurement precision was ± 2.0 μmol/kg (Park et al., 2008).

The injected CO<sub>2</sub> concentration (C<sub>0</sub>) was measured on water samples collected from the surface holding tank, after CO<sub>2</sub> bubbling but just before injection, using a TOC-IC analyzer (total organic carbon-inorganic carbon, Teledyne Termar Inc.) at Pusan National University. Dissolved CO<sub>2</sub> in each sample was gasified by adding 1 M H<sub>2</sub>SO<sub>4</sub>

solution until  $\text{pH} < 2$  and then the gasified  $\text{CO}_2$  was carried by  $\text{NO}_2$  gas (gas flow-rate: 200 mL/min) and the  $\text{CO}_2$  concentrations were determined using a non-dispersive infrared detector (NDIR).

$\text{pCO}_2$  values were not measured directly, but rather were modelled with the program PHREEQC (Parkhurst and Appelo, 2013) using the input parameters of alkalinity, pH, temperature, and major cation and anion concentrations. Theoretical TIC values of  $\text{CO}_2$ -saturated solutions under different temperature and pressure conditions were also estimated with this program.

### 3.5. Mass balance analysis of $\text{CO}_2$ leakage

The high  $\text{CO}_2$  partial pressure of the injected fluid drives  $\text{CO}_2$  degassing until equilibrium in the shallow aquifer system is achieved via partitioning between the injected fluid and free  $\text{CO}_2$  gas. The concentration of  $\text{CO}_2$  in groundwater is, however, a complex function of chemical, biological and physical processes, and thus changes in  $\text{CO}_2$  distribution will not be solely related to degassing. The degassing loss of  $\text{CO}_2$  can be indirectly constrained using other gases, such as the biochemically inert noble gases, that partition into the newly formed  $\text{CO}_2$  bubbles (Gilfillan et al., 2008; Györe et al., 2017). Since the partitioning coefficients of elements at the gas-liquid interface are proportional to their mass, this process can lead to mass dependent fractionation.

To quantify the amount of degassed  $\text{CO}_2$ , it is necessary to focus on the fate of  $\text{CO}_2$  bubbles after the phase-partitioning process. Depending on the mobility of the  $\text{CO}_2$  bubbles, a system is defined as either open or closed (Ma et al., 2009). In a closed system, the  $\text{CO}_2$  bubble is retained in the groundwater and thus equilibrium between the  $\text{CO}_2$  bubble and the surrounding  $\text{CO}_2$  plume is achieved. In an open system, there is a continuous loss of  $\text{CO}_2$  bubbles until the end of the phase-partitioning process. With continuous degassing, the noble gas composition of the dissolved plume is gradually enriched with heavier elements (Holland and Gilfillan, 2013; Zhou et al., 2005). The degassed mass can be constrained iteratively and inversely using different noble gases (Ballentine et al., 2002; Holland and Gilfillan, 2013). A detailed description of the analytical approach used in this paper is given in Appendix A and B.

## 4. Results

### 4.1. Background groundwater before injection

Pressure and temperature variations at the test site could be a driving force for degassing of the injected partitioning tracers (Sakaki et al., 2013). At the K-COSEM test site, changes in groundwater level prior to  $\text{CO}_2$  injection correspond to changes in atmospheric pressure and not to human activities such as groundwater pumping (see Figure SM-1 in Supplementary Material). Groundwater temperatures correspond to normal seasonal values (12.9–13.7°C).

Three components of the carbonate system ( $\text{pCO}_2$ ,  $\text{HCO}_3^-$ , pH) and dissolved oxygen (DO) were monitored for about 10 months prior to the injection experiment (Fig. 4); note that only one TIC sample was collected prior to injection due to laboratory availability. The  $\text{HCO}_3^-$  values are between 41.1–93.0 mg/L, pH is between 6.2–6.7, and calculated  $\text{pCO}_2$  ranges from 0.01–0.03 atm (Fig. 4); these values are likely linked to the presumed low carbonate levels in the biotite granite protolith. DO shows a general increasing trend from about 4 to 7 mg/L in wells IW and SMW 2-2 prior to injection while values in PS-04 and, especially, BS-09 are more irregular.

Noble gas baseline concentrations measured in boreholes (BH) 01 to 05 (Table 1) show a narrow range (see standard deviations) and values typical of shallow groundwater systems. The baseline results from the borehole closest to the injection well (BH-04) are plotted as a reference level in various figures below (Figs. 7, 9, 10 and 11).

### 4.2. Injection of gas-infused groundwater

The  $\text{CO}_2$ -infused groundwater had a measured  $\text{CO}_2$  concentration of 76.87 mM prior to injection, which is very similar to the theoretical saturation values calculated using PHREEQC (Parkhurst and Appelo, 2013) assuming surface conditions of  $T = 2^\circ\text{C}$  and  $\text{pCO}_2 = 1\text{--}1.1$  atm (considering the water column in the tank). The He and Kr concentrations measured in this same solution were  $3.12\text{E-}06$  cm<sup>3</sup> STP/g and  $4.04\text{E-}06$  cm<sup>3</sup> STP/g, respectively. Unfortunately, there is no data for Ar concentration in the chaser fluid prior to injection, and thus initial Ar was estimated to be  $2.59\text{E-}02$  cm<sup>3</sup> STP/g based on the initial maximum concentration in the injection well. These values are below the solubility levels for the *in-situ* conditions and thus the noble gases will stay in solution unless put in contact with a low partial pressure atmosphere (such as the vadose zone) or bubbles.

Water level (WL), temperature (T), and electrical conductivity (EC) values in the injection well (IW) show a clear difference between the two injected fluids (Fig. 5a), with intermediate values for the initial  $\text{CO}_2$ /Kr/He – charged fluid and slightly higher WL and lower T and EC values for the subsequent Ar-charged chaser fluid. During the injection period, WLs increased then decreased rapidly in all observation wells (Fig. 5b–f), showing maximum rises from 0.45 to 0.2 m (SMW2-2 > SMW 2-3 > PS-04 > BS-09 > SMW 2-1) as a function of their horizontal distance and depth relative to the IW. The form of the pressure response is essentially the same in all wells except for the slower rise and fall in SMW 2-1. All observation wells show some change in T and/or EC values during the injection period that generally re-stabilized immediately afterwards (Fig. 5b–f). Over the following three months, the WLs in all wells slowly decreased at the same rate as a function of seasonal effects (Fig. 5g–l). In the IW, T and EC recovered to pre-injection levels after about 1 month and 1 week, respectively (Fig. 5g). During this longer monitoring period, small drops in temperature (0.1–0.3°C) were observed in wells BS-09 (27/12/2016), SMW2-1 (2/12/2016), SMW 2-2 (5/12/2016), and SMW 2-3 (7/12/2016) (Fig. 5h–l). The EC data is noisier and generally does not show any clear trend, aside perhaps from the increase observed in BS-09 that corresponds with a T change around 27/12/2016 (Fig. 5h).

Over the first 20 days of the experiment there was noticeable variation in IW data, such as a 5-fold increase in TIC, a 1 unit drop in pH, and a 50% drop in DO (Fig. 6a). During this same period, the response of TIC and pH in three of the observation wells is generally similar (Fig. 6), with a clear change in trend occurring around 4 days after injection (3/12/2016). Over the following three months, the values for these and other carbonate system parameters in the IW trended towards pre-injection conditions, although both pH and  $\text{pCO}_2$  remained lower and higher, respectively (Fig. 4a). In the observation wells, various changes in the carbonate system indicated a variable, and sometimes complex breakthrough of the two injected fluids: BS-09 shows the simplest and largest change in trend for numerous parameters, with an increase in TIC,  $\text{HCO}_3^-$ ,  $\text{pCO}_2$  and decrease of pH around 27/12/2016 (Fig. 4b). PS-04 shows less pronounced changes, aside from a small pH and DO peak in the weeks after injection (Fig. 4c). Finally, SMW 2-2 shows an initial period of change to 21/12/2016 (e.g. decreasing TIC and increasing pH) followed by stable values to 24/1/2017, while samples taken at the end of the monitoring period (23/2/2017) appear to show a decrease in pH and increase in TIC (Fig. 4d). The DO results in the observation wells are less conclusive over this period, although a significant drop from 6.7 mg/L on 1/12/2016 to 2.1 mg/L on 5/1/2017 occurs in SMW 2-2.

Noble gas tracers also show clear variations from their baseline values following the injection event when plotted together for each individual gas (Fig. 7). This same data can, instead, also be plotted as breakthrough curves for each individual well (Fig. 8). Here, the noble gas data are given as  $C/C_0$ , where  $C = (\text{sampled concentration} - \text{ASW concentration})$  and  $C_0 = (\text{maximum IW concentration} - \text{ASW concentration})$ . Plotting values against the initial source concentration

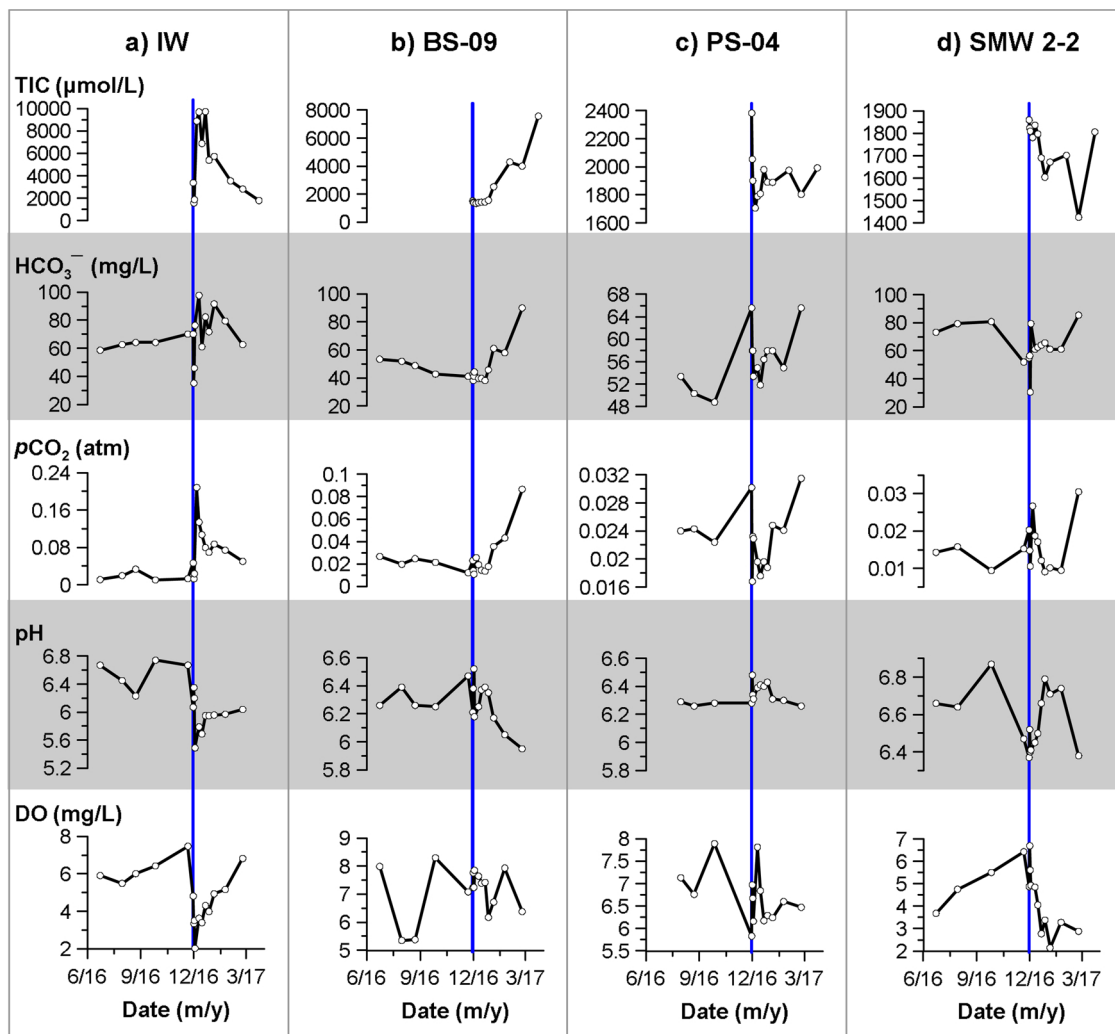


**Fig. 4.** Measured TIC,  $\text{HCO}_3^-$ , pH and DO, and modelled  $p\text{CO}_2$  values at four selected wells. Only 6 of the total 10 months of baseline monitoring are shown in this figure for clarity. The vertical blue line marks the injection period. Note the different arrival times in the observation wells, in particular the later arrival in well BS-09 (b) and earlier, but less-pronounced arrival in PS-04 (c) closer to the injection period. Only one TIC sample was collected from the IW before injection because of laboratory availability.

**Table 1**

Noble gas concentrations measured from the five BH-series wells before  $\text{CO}_2$  injection.

Well	He ( $\times 10^{-8}$ )	Ne ( $\times 10^{-7}$ )	Ar ( $\times 10^{-4}$ )	Kr ( $\times 10^{-7}$ )	Xe ( $\times 10^{-8}$ )
ASW <sup>†</sup>	4.58	1.96	3.59	0.83	1.20
BH-01	6.49	2.86	4.23	0.94	1.31
BH-02	6.17	2.64	4.64	1.08	1.42
BH-03	7.15	3.02	5.23	1.18	1.58
BH-04	6.19	2.64	3.93	0.85	1.06
BH-05	8.91	3.95	4.87	1.02	1.40
% std dev. <sup>‡</sup>	16.4	18.0	11.2	12.5	14.1

Concentration is given as volume of gas per gram of water (i.e.  $\text{cm}^3$  STP/g), where STP is defined as standard temperature and pressure after Ozima and Podosek (2002) ( $p = 0.101$  MPa,  $T = 0^\circ\text{C}$ ).

<sup>†</sup> Air Saturated Water was calculated based on the groundwater conditions ( $13.2^\circ\text{C}$ ,  $0.101$  MPa and salinity of  $0.01$  g/kg).

<sup>‡</sup> 1 sigma value of five samples relative to the average, in percent.

normalizes the data, while subtracting the ASW value means that negative values (shown by unfilled symbols) represent concentrations less than background air saturated water levels. Note that the Fig. 8 plots also show the breakthrough of TIC, which is often very similar to that of the noble gases (especially TIC-Kr).

The first noble gas concentrations measured in the injection well (IW) (Fig. 7) are lower than those measured on the surface, but to a different extent for each gas:  $3.65\text{E-}07$   $\text{cm}^3$  STP/g for He (12% of

surface value) and  $1.86\text{E-}06$   $\text{cm}^3$  STP/g for Kr (46%). Both He and Kr show wide variability in the IW during the early phases of the experiment (Fig. 8a), with a high initial value followed by low values near or below the AWS level. Concentrations then stabilize at moderately high values for a period of about 17 days (December 10th to 27th) before decreasing towards the end of the monitoring period. During this final phase their trends deviate slightly, with Kr decreasing more rapidly than He. The behavior of Ar, injected with the chaser fluid, differs from

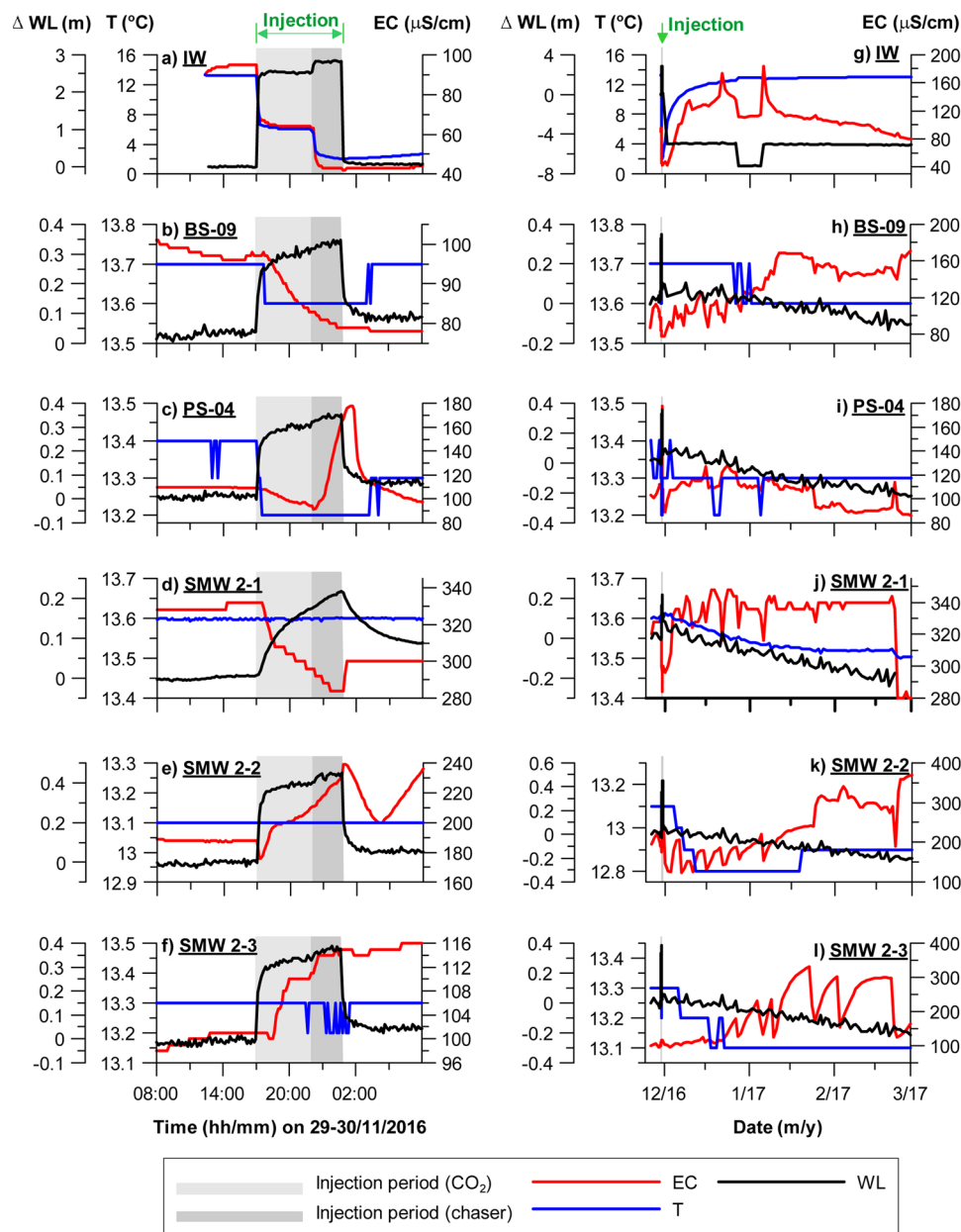


**Fig. 5.** Water level (WL), temperature (T) and electrical conductivity (EC) changes measured *in-situ* in the monitoring wells. The plots on the left show the 24-h period straddling the injection, highlighting the distinct signatures of the two injected fluids (a) and the rapid response of the measured parameters in the observation wells (b–f). The plots on the right present all collected data, showing the time required to return to pre-injection values in the IW (g) and a second, later arrival of injected fluids in some wells (h, k, l). The injection period is highlighted by a vertical grey box or line in all figures.

the other two gases. Ar starts with a moderate value that increases earlier and remains high for about 10 days (December 1st to 10th), followed by a rapid decrease and then a slower decrease that matches that of He.

Noble gas concentrations measured in the observation wells are lowest in PS-04, and generally intermediate for SMW 2-2 and highest for BS-09 (Fig. 7). The maximum concentrations observed in BS-09 are about 31% of the maximum IW value for He, 24% for Kr, but only about 14% for Ar. In PS-04 (Fig. 8b), the first sample on 30/11/2016 shows higher Kr and Ar concentrations followed by low values near the ASW line for the duration of the experiment. In SMW 2-2 (Fig. 8c), the values prior to 27/12/2016 are near, or in the case of He much below, the ASW line, other than a very small peak for all three gases in the second sample on 2/12/2016. After 27/12/2016, the values rise, although Kr and Ar follow a similar, step-wise increasing trend compared to the more regular increase observed for He. The results from BS-09 (Fig. 8d)

are the only ones that show a clear difference in breakthrough times between the co-injected He and Kr (between 10/12/2016 and 27/12/2016) compared to the later injected Ar (sometime after 5/1/2017).

## 5. Discussion

### 5.1. Fluid mixing and migration

The two injected fluids had distinct chemical characteristics after preparation. The first (i.e. CO<sub>2</sub> fluid) had high pCO<sub>2</sub>/TIC/He/Kr and low Ar/pH, while the second (i.e. chaser fluid) had high Ar/pH and low pCO<sub>2</sub>/TIC/He/Kr; both solutions had low O<sub>2</sub>, EC and T. The low concentrations of Ar/O<sub>2</sub> in the first solution and He/Kr/O<sub>2</sub> in the second were likely the result of stripping caused by bubbling the pure gases during solution preparation, while the same mechanism likely caused the slight TIC and EC decrease and pH increase in the second solution

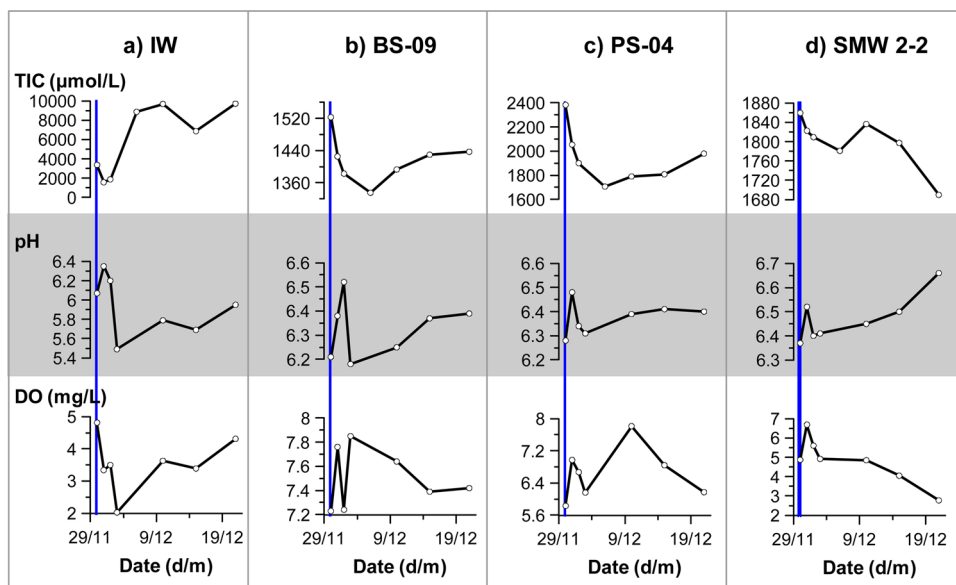


**Fig. 6.** TIC, pH, and DO values observed in the IW (a) and three observation wells (b–d) during the first 20 days of the injection experiment. Note the significant differences between the TIC and pH scales for the different wells and that TIC sampling was sometimes conducted on different days. The vertical blue line defines the injection period.

due to stripping of background CO<sub>2</sub>. The low EC values in the first solution were likely due to the fact that most inorganic carbon would be in the neutral H<sub>2</sub>CO<sub>3</sub><sup>\*</sup> form under the associated low pH conditions. The low water temperatures in both solutions were due to environmental conditions during preparation.

During injection, it is assumed that some mixing would have occurred between the first solution and the background groundwater and then between the second and first solutions, thus creating a range of fluids that are intermediate between the three end-members. A roughly concentric distribution of these end-member and mixed fluids likely formed in the vicinity of the IW due to a radial gradient induced by piezometric mounding. Once injection stopped, this distribution would be transported laterally (with continued dispersion and mixing) via the local, pre-injection groundwater flow direction(s). As discussed below, these conditions resulted in different breakthrough behaviors at the various, closely spaced observation wells as a function of their relative locations.

This spatial zonation can be seen in the early IW data. During

injection itself, EC and T clearly define the two injected fluids (Fig. 5a) with relatively rapid displacement of fluids (about 1.5 h) and limited borehole mixing. Data collected over the following week show the early presence of the chaser fluid (low pCO<sub>2</sub>/TIC/He/Kr and high Ar/pH) followed by re-entry of the CO<sub>2</sub> fluid (high pCO<sub>2</sub>/TIC/He/Kr and low pH, high TIC) into the IW (Figs. 6a and 8a). Over the longer term, values trended towards background levels in the carbonate parameters (Fig. 4a) and noble gases (Fig. 8a). The overall behavior of the different solutions in the IW are best illustrated using a ternary plot of the conservative noble gas tracers (Fig. 9). This figure shows a significant difference between the composition of the first injected fluid and the first collected sample, which may be due to initial CO<sub>2</sub> degassing related to the higher subsurface temperatures (see Section 5.2 below). The composition of the second sample is very similar to that of the subsequently injected chaser fluid, followed by seven samples that plot on a mixing line between the first and second samples. The trend then changes abruptly and shifts towards background concentrations for the last two samples, implying that the concentric distribution described above has

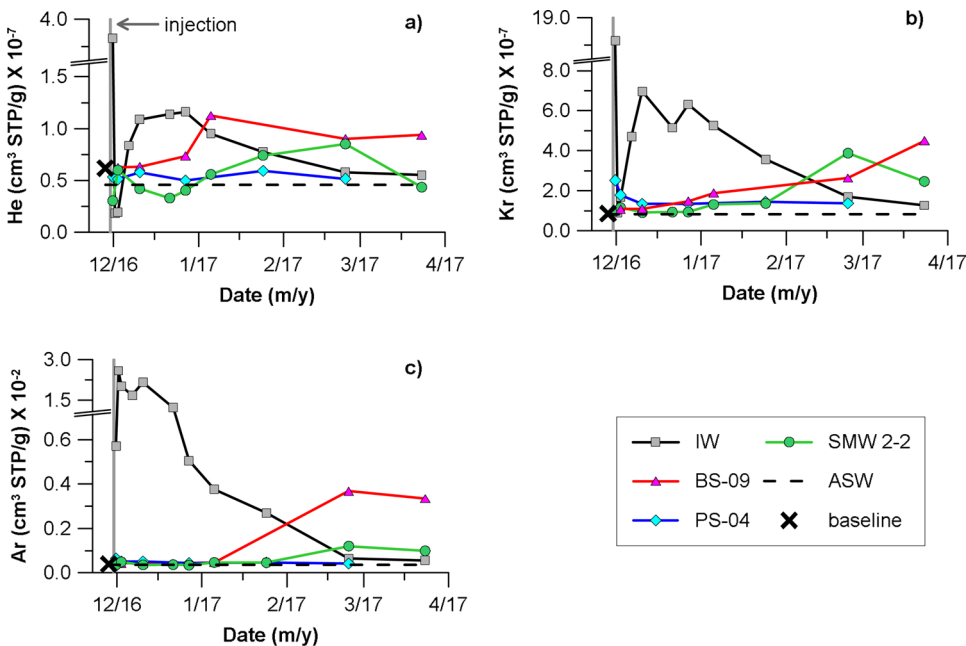


**Fig. 7.** Measured noble gas concentrations in the IW and three selected observation wells. Baseline values were measured in the nearby borehole BH-04 in March 2015 and are plotted just prior to the injection experiment for reference. Air Saturated Water (ASW) values were defined (Kipfer et al., 2002) based on an average groundwater temperature of 13.2°C, 0.101 MPa and salinity of 0.01 g/kg. The vertical grey line in each plot represents the injection period. Note the similar He and Kr trends, but different Ar trend, in the IW as a function of the two different injection fluids, which also influences the breakthrough times and behaviors observed in the other wells.

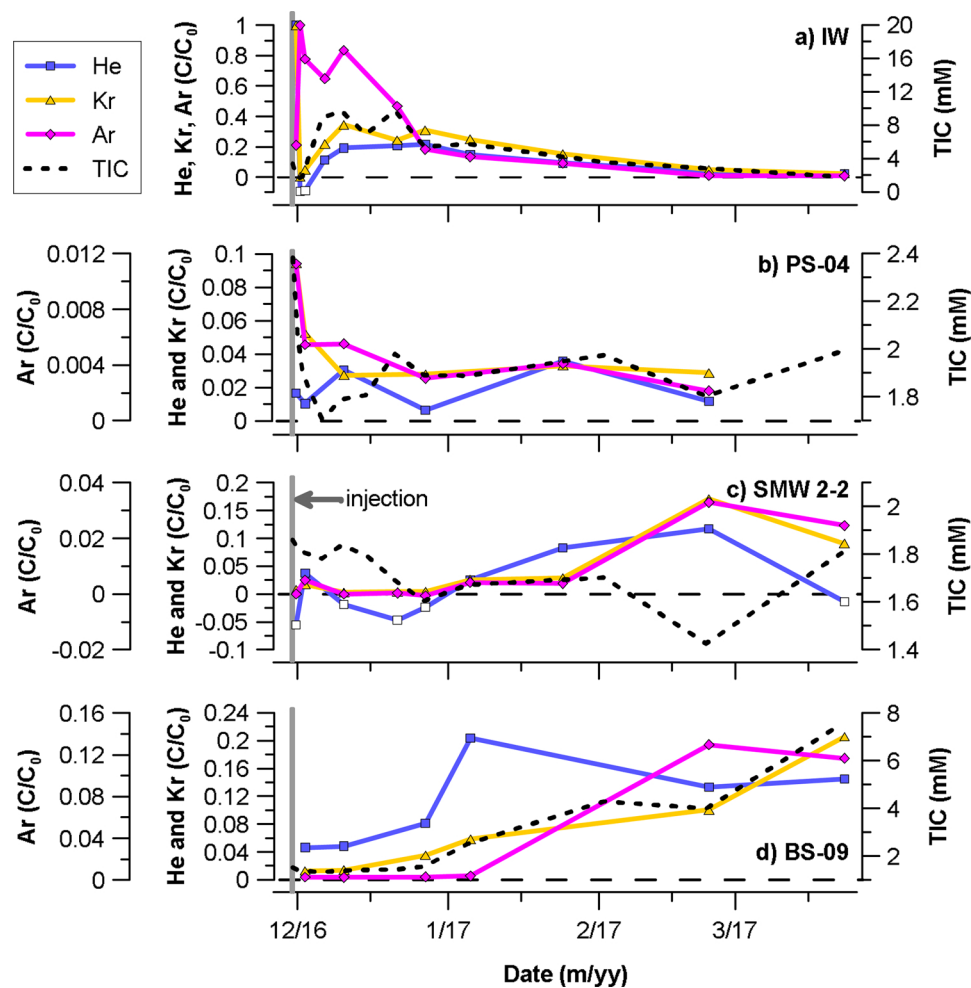


**Fig. 8.** Observed temporal evolution of the three noble gas tracers at each well, presented as  $C/C_0$  for each individual gas, together with total inorganic carbon (TIC) for reference. The dashed horizontal line at “0” separates values greater than or less than ASW levels, while the vertical grey line represents the injection period. Note the different behaviors of the two injection fluids in the IW (a), the early time peak coincident with injection at the up-gradient well PS-04 (b), the initial negative He values and subsequent moderate peak in SMW 2-2 (c), and the later but well-defined breakthrough at BS-09 (d).

been swept past the IW along the natural groundwater gradient.

The fact that almost all observation wells show a similar and very rapid pressure response in correspondence with the start and end of injection (Fig. 5b–f), with relatively little delay/tailing, highlights the good hydraulic connectivity between the wells. In addition, EC changes in all observation wells and very small temperature changes in two wells (Fig. 5b–f) during injection, measured every 10 min with the LTC probes, imply that forced, higher-gradient radial flow during injection may have resulted in the very early arrival of a small amount of injected fluid. Considering the highly anisotropic conditions around the injection zone (Lee et al., 2017a,b; Kim, 2017; Kim et al., 2018), there is the potential that heterogeneous permeability distributions provided a fast, preferential-flow pathway for a small portion of the  $\text{CO}_2$ -rich plume (Kilgallon et al., 2018; Lu et al., 2012).

Less frequent manual sampling of other parameters also shows changes in the observation wells during the first couple of days of monitoring that appear to be linked with injection. For example, BS-09, PS-04, and SMW 2-2 all show a pH peak and decreasing TIC values during the first 4 days after injection followed by a more gentle increasing trend for the subsequent 4 days, similar in form to that observed in the IW (Fig. 6). Some of the observation wells also show noble gas variations during this early period, although slightly different sampling times mean that a direct comparison is difficult. For example, PS-04 and SMW 2-2 both show small peaks soon after the injection period (Fig. 8b, c), with the latter corresponding with a clear  $0.3^\circ\text{C}$  drop

in temperature (Fig. 5k). This rapid response is likely due to the fact that both wells lie within the radius of influence around the IW (Fig. 1), calculated to be 2.9 m assuming an effective porosity of 0.02 (based on previous push-drift-pull tests; Kim, 2017 and Kim et al., 2018), concentric flow and distribution, and an aquifer thickness of 14 m. Over the longer term, the three observation wells behave differently based primarily on their position relative to the IW and the natural background flow direction, as described below.

In general, PS-04 showed the lowest levels for most measured parameters, with small, early-time anomalies decreasing rapidly towards baseline concentrations for carbonate system variables (Fig. 4c) and noble gases (Fig. 8b). This implies that PS-04 experienced breakthrough during injection-induced radial flow, but that these injected fluids were then immediately swept away due to a return to baseline flow directions (possibly NW to SE, Fig. 1) that re-introduced background groundwater. This interpretation is supported by the PS-04 trend in Fig. 9, where values start in the vicinity of the initial IW sample and then trend towards background levels during the rest of the experiment.

The most complex behavior is observed in SMW 2-2. The gentle but significant drop in DO values over the entire monitoring period (Fig. 4d) implies that this well always contained some portion of the injected fluids. The initial rise in pH and drop in TIC up until 27/12/2016 indicates the presence of the chaser fluid (Fig. 6d), which is supported by He values below the ASW level (i.e., degassed during

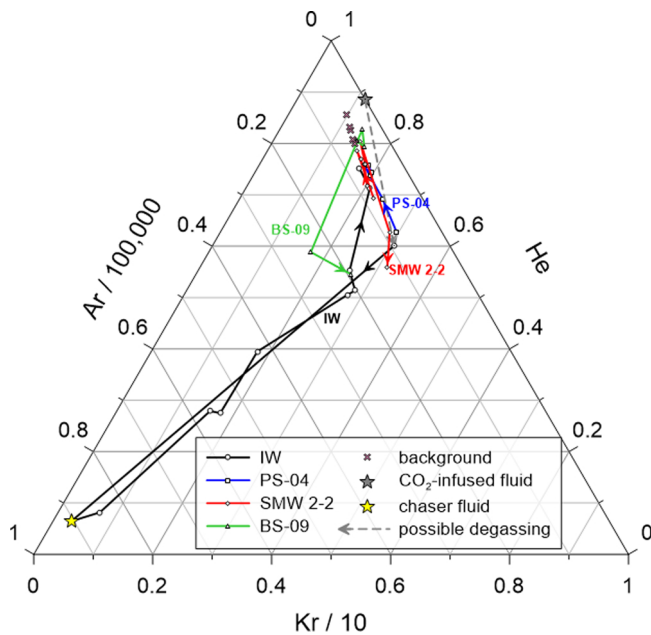


**Fig. 9.** Ternary plot showing the temporal variation of fractional abundance of Ar, Kr, and He species in the four wells. Arrows indicate the temporal order of the various samples. Background values are those collected in BHs 01-05. The noble gas concentrations in the “CO<sub>2</sub>-infused fluid” were measured on samples collected from the holding tank before injection, while those in the “chaser fluid” were measured on the first sample collected from the IW immediately after injection had ceased. The straight line trends between different end-member compositions imply mixing as the plume migrates via both the initial forced gradient and the subsequent recovery of the natural gradient.

chaser fluid preparation) (Fig. 8c) and occurrence of these samples on the mixing line with the Ar chaser fluid (i.e. pink squares in Fig. 10). Subsequently, a small drop in pH during January 2017 followed by a large drop before 23/2/2017 indicates the arrival of the CO<sub>2</sub>-infused fluid (Fig. 4d); this is supported by a very similar inverse trend for Kr

and a final noble gas composition that is very similar to the first IW sample (Fig. 9). These complex trends are likely due to both the close proximity and down-gradient location of this well relative to the IW, which resulted in passage over time of different sections of the zoned plume described above.

In contrast, the long-term monitoring results from BS-09 are more straightforward, as this well has the largest measured anomalies as well as the separate breakthrough of two distinct fluids that maintained some characteristics of the two original injection solutions. The arrival of the initially injected CO<sub>2</sub>-infused fluid occurs between 21/12/2016 and 27/12/2016 with a sharp rise in TIC, HCO<sub>3</sub><sup>-</sup>, pCO<sub>2</sub> and drop in pH (Fig. 4b) and a small drop in T and increase in EC (Fig. 5h). Kr and He also rise at this time and there appears to be a good correlation with TIC (Fig. 8d), although the lower sampling frequency for the noble gases results in a wider potential arrival window (10/12/2016 to 27/12/2016). The breakthrough of the chaser fluid is shown primarily by the significant increase in Ar, which, due to the low sampling frequency during this period, can only be roughly defined as between 5/1/2017 and 23/2/2017. This behavior is also illustrated in the noble gas ternary plot (Fig. 9), with the final values trending towards the main mixing line observed in the IW. In terms of flow, the two arrivals indicate the lateral movement of the concentrically distributed fluids along the natural groundwater gradient (made simpler by the greater distance of this well) while the fact that the highest anomalies were observed here indicate preferential movement between the IW and BS-09. Both processes are conditioned by local permeability anisotropy (Lee et al., 2017a), similar to that observed by Lu et al. (2012).

It is interesting to note that the noble gas behavior observed in this experiment relative to the migrating CO<sub>2</sub>, as illustrated in Fig. 8, is different from some experiments reported in the literature. Here, the Kr and TIC breakthrough times were very similar and He showed the fastest movement amongst the indicators, particularly clearly in BS-09 (Fig. 8d) and moderately in the second peak of SMW 2-2 (Fig. 8c). This is in contrast to the observation by Kilgallon et al. (2018) that all noble gases migrated faster than CO<sub>2</sub>, and that Kr preceded He, in laboratory experiments, and the observation by Carrigan et al. (1996) and Sanford et al. (1996) that the retardation of He was noticeable compared to other tracers in a field experiment. The lack of retardation of He in

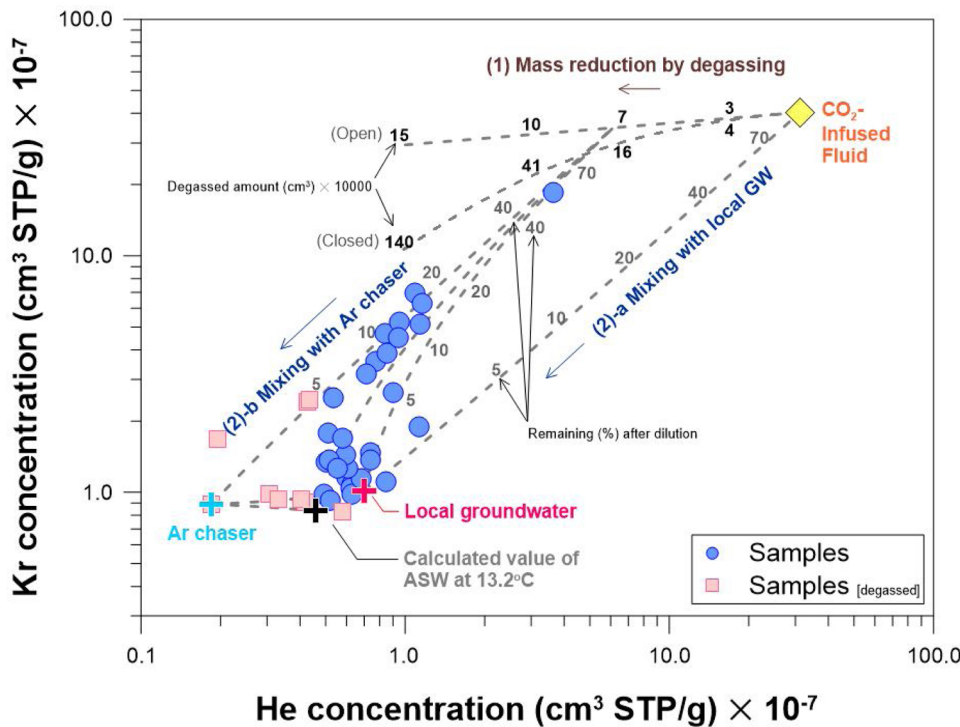


**Fig. 10.** He-Kr plot showing mass balance of the plume. The un-degassed groundwater follows the mixing line between injected (yellow diamond) and background concentration (pink cross). The new dilution line follows the mixing line of partially degassed groundwater (at the intercept between ⊕ and ⊖-b) with background concentration (pink/black cross) or Ar chaser (light blue cross). The pink squares represent significantly degassed samples below Air Saturated Water (ASW) concentration (Fig. 8). The local groundwater represents the background concentration before CO<sub>2</sub> injection event.

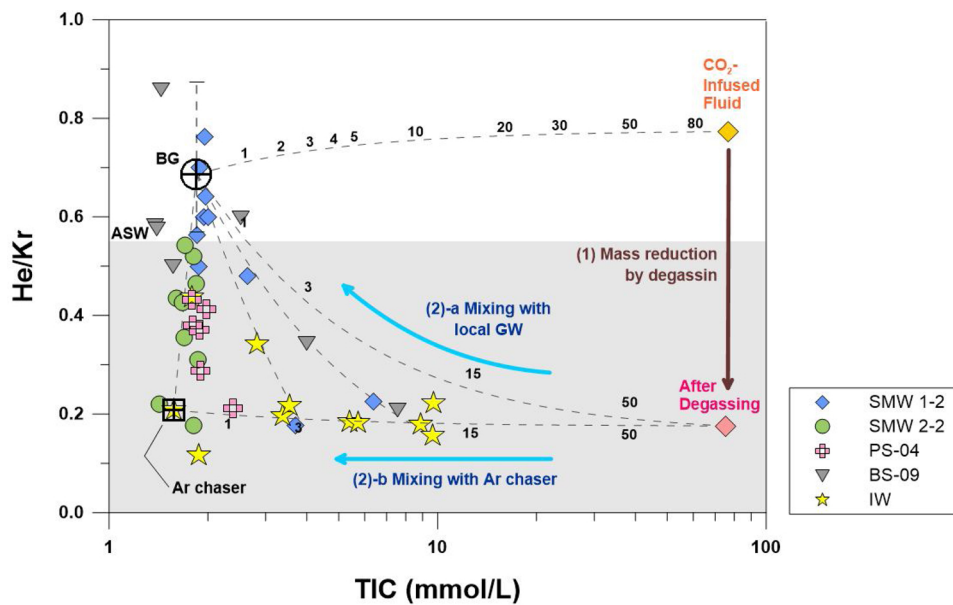


Fig. 11. Plot showing the He/Kr ratio versus TIC for five wells. Following the degassing event the noble gas ratios are enriched in heavier species relative to the Air Saturated Water (ASW) line. The pink diamond corresponds to the intercept between the degassing and dilution lines in Fig. 10. Most samples follow the mixing line between the three components of CO<sub>2</sub> plume (after degassing), chaser fluid (Ar chaser) and local background groundwater (BG), indicating that degassing and dilution process are responsible for the sample distribution.

these results, attributed in other experiments to rapid movement of this gas into immobile zones, may give information on the permeability distribution in this aquifer, however more study would be required to address this issue. Another factor which could also contribute to the different observed behaviors could be the different experimental scales (lab versus field) and the permeability and porosity characteristics and heterogeneity of the studied porous media. Consequently, in terms of fast and efficient leakage detection, the best monitoring parameter may be site-specific, apparently even amongst the noble gas tracers.

Finally, the dissolved CO<sub>2</sub> plume does not appear to have migrated upward towards the water table until four months after the injection stopped, as prior to this no significant change in  $p\text{CO}_2$  ( $< 1$  atm) was detected in the shallowest monitoring wells (e.g. SMW 2-1, data not shown). In addition, the lack of CO<sub>2</sub> anomalies in the unsaturated zone monitoring wells (Fig. 4.8.4.29 in KMOE, 2017) imply that the injected plume was retained in the groundwater without diffusive loss towards the atmosphere. It is likely that the current experimental conditions (e.g. injection amount, monitoring period) were insufficient for aqueous-phase CO<sub>2</sub> to migrate diffusively through the 4 m of overlying saturated soils (i.e., between the minimum injection depth and the piezometric surface).

## 5.2. Assessment of degassing

The carbonate system and noble gas results in the observation wells suggest that injected mass was conserved during transport after the plume left the injection point, as CO<sub>2</sub> was diluted below the saturation point ( $p\text{CO}_2 < 1$  atm). However, the noble gas ratio of sampled groundwater did not belong to the mixing range between injected fluid (He/Kr = 0.77) and local groundwater (He/Kr = 0.69), but rather it had a newly fractionated ratio of 0.18 (Fig. 10). Since mixing cannot account for such a strong fractionation, another physical process, degassing, was considered to explain the enrichment of injected tracers. Gilfillan et al. (2017) incorporated three distinct components to evaluate the fate of the CO<sub>2</sub>-infused fluid: (i) injected fluids; (ii) fluids produced from shallow groundwater after the injection event; and (iii) undisturbed groundwater that has a background concentration before CO<sub>2</sub> injection. These end-members were used here to constrain the various physical processes causing noble gas anomalies, such as dilution with local groundwater and degassing.

Although the first injected solution was saturated with CO<sub>2</sub> under the conditions on surface, its injection into the subsurface exposed it to

temporally and spatially variable temperatures and pressures that could have a strong impact on CO<sub>2</sub> solubility. For example, pressures over the 3 m injection interval were 1.4–1.75 atm under normal hydrostatic conditions and 1.7–2.05 atm during the injection phase due to piezometric mounding (Fig. 5a), while temperatures increased over time as the 2°C injected water was warmed to the *in-situ* temperature of 13.2°C. CO<sub>2</sub> solubility was modelled for these conditions using PHREEQC (Parkhurst and Appelo, 2013) (see Supplementary Material). During the injection period the first solution was always found to be undersaturated with CO<sub>2</sub> due to the higher pressures, regardless of the temperature, and thus in-well degassing was not possible. In contrast, after the injection period, when water levels returned to natural values, the solution becomes oversaturated over a range of conditions between 9.5–13.2°C and pressures less than 1.58 atm (i.e.,  $< 22.8$  m depth). As such, degassing was thermodynamically possible under these conditions. The maximum level of oversaturation, at 13.2°C and a depth of 21 m (assuming the plume did not rise above the upper injection interval) was about 111%.

As degassing is rapid, we assume that it occurred close to the IW before significant mixing with the chaser fluid and the local groundwater (Fig. 10). This CO<sub>2</sub> degassing would drive changes in the initial noble gas ratios, as the lighter noble gases preferentially partition into the CO<sub>2</sub> bubbles. Based on the change of noble gas composition, the degassed CO<sub>2</sub> volume was quantified using the following assumptions: (i) degassing loss was terminated at the start of groundwater transport; (ii) the ideal gas law was satisfied (hence, Dalton's law); and (iii) the produced CO<sub>2</sub> bubbles were at 1 atm.

The calculation was made iteratively and inversely, starting from an initial guess on a degassed volume ( $V_g$ ), to obtain the  $m_{\text{NG1}(l)}$  and  $m_{\text{NG2}(l)}$  ratio of monitored data in the field:  $\left(\frac{m_{\text{NG1}(l)}}{m_{\text{NG2}(l)}} = \frac{\text{He}}{\text{Kr}}\right) \rightarrow 0.18$  (see 3.5 Mass balance analysis of CO<sub>2</sub> leakage). Following CO<sub>2</sub> degassing, He was reduced from 3.12E-06 cm<sup>3</sup> STP/g to 4.67E-07 cm<sup>3</sup> STP/g (-85.0% in total) and Kr was reduced from 4.04E-06 cm<sup>3</sup> STP/g to 2.66E-06 cm<sup>3</sup> STP/g (-34.2% in total) considering a closed system, and He was reduced to 6.12E-07 cm<sup>3</sup> STP/g (-80.4% in total) and Kr was reduced to 3.48E-06 cm<sup>3</sup> STP/g (-13.9% in total) considering an open system. The notable difference of Kr concentrations in the two systems is due to stepwise degassing in an open system, where the heavier Kr is gradually enriched during the multi-step process. The total amount of degassed CO<sub>2</sub> was estimated to be 0.529 kg (3.1%) considering a closed system and 0.156 kg (0.9%) considering an open system, from a total injected mass of 16.9 kg. Following the degassing, the newly formed end-

member was continuously mixed with the chaser fluid and local groundwater, driving dilution towards a He/Kr ratio of 0.69 during transport (Fig. 10).

In contrast to the chemically inert noble gases, CO<sub>2</sub> is known to have higher and more variable background concentrations because of the diverse chemical and biological processes that generate and consume CO<sub>2</sub> in groundwater systems (e.g., Macpherson et al., 2008; Vesper and Edenborn, 2012). The relationship between CO<sub>2</sub> (in the form of TIC) and the inert tracers of He and Kr is presented in Fig. 11. The initial plume first degasses the CO<sub>2</sub> bubbles, leaving the water enriched in the heavier Kr species such that they plot below the ASW ratio line while the TIC values barely change (brown vertical line). Subsequently, most samples lie on the physical mixing lines between the degassed plume, Ar-chaser and local groundwater (BG). These trends indicate that degassing and physical mixing are the major process responsible for the CO<sub>2</sub> plume evolution. On the other hand, a few samples do not exhibit any correlation with TIC, which could be attributed to: (i) biochemical sources and sinks controlling the CO<sub>2</sub> distribution; (ii) significant degassing of noble gases at the plume head and tail; and (iii) the higher diffusivity of noble gases relative to CO<sub>2</sub> and thus longer transport distances of the noble gases (Kilgallon et al., 2018; Stanley and Jenkins, 2013).

## 6. Summary and conclusions

A relatively small amount of CO<sub>2</sub> saturated groundwater spiked with He and Kr tracers was injected into a shallow aquifer to simulate minor CO<sub>2</sub> leakage into a highly anisotropic hydrogeological setting, followed by injection of a chaser solution charged with Ar. Noble gas tracers and a wide range of other physical-chemical parameters were used to interpret flow between the closely spaced observation wells over the 4 month long experiment, and then the noble gas data were used to constrain a mass balance model of CO<sub>2</sub> degassing.

The two injected fluids were distinct, the first defined by high pCO<sub>2</sub>/Kr/He and low O<sub>2</sub>/Ar/T/EC and the second by high Ar and low pCO<sub>2</sub>/O<sub>2</sub>/Kr/He/T/EC. Initial radial flow during injection, due to water table mounding, was recognized in observation well data from *in-situ* loggers, with rapid pressure changes showing good hydraulic connectivity and small T and EC anomalies implying the occurrence of fast, preferential-flow pathways for a small portion of the injected plume during induced, high-gradient, injection-phase conditions. Changing hydraulic conditions were shown by the early arrival of noble gases and carbonate system parameters in an up-gradient well immediately after injection that was followed by a rapid return to background values as the pre-injection gradient was quickly re-established. This flow regime eventually led to the clear and distinct breakthrough of the two injected fluids at a more distant, down-gradient well. The initial arrival of the CO<sub>2</sub>-infused solution in this well was marked by the arrival of elevated

## Appendix A. Analytical solutions for leaking CO<sub>2</sub> mass balance

To quantify the mass of degassed CO<sub>2</sub> it is necessary to focus on the fate of CO<sub>2</sub> bubbles produced during the phase-partitioning process. Depending on the mobility of the CO<sub>2</sub> bubbles, a system is defined as either open or closed. In a closed system, the CO<sub>2</sub> bubble is retained in the groundwater and thus equilibrium between the CO<sub>2</sub> bubble and the surrounding CO<sub>2</sub> plume is maintained. The analytical solution for closed system degassing is a one-step phase-partitioning process following Henry's law (Sander, 2017):

$$\left(\frac{A}{B}\right)_{(g)} = \left(\frac{A}{B}\right)_{(l)} \alpha$$

$$\alpha = \frac{\frac{r_A}{\phi_A} K_A \text{ (atm/M)}}{\frac{r_B}{\phi_B} K_B \text{ (atm/M)}}$$

where:

- $\left(\frac{A}{B}\right)_{(g)}$  = A and B ratio in CO<sub>2</sub> bubbles, where A and B are different noble gases
- $\left(\frac{A}{B}\right)_{(l)}$  = the composition of A and B remaining in the dissolved phase
- $\alpha$  = partitioning coefficient for gas/liquid system

TIC/Kr/He values, with the particularly good association between the first two species implying limited chromatographic separation (at least at the temporal resolution of the sampling). Arrival of the chaser fluid was observed shortly after with increasing Ar concentrations.

In terms of the physical processes acting on the injected fluids, the monitoring data show a strong enrichment of heavier noble gases (i.e. decrease in the He/Kr ratio) that cannot be explained by dilution of the injection fluid with local groundwater. Rather, the enrichment originates from CO<sub>2</sub> degassing driven fractionation of the noble gas elemental ratios, with degassing being induced by local temperature and pressure conditions in the subsurface. In fact, in contrast to deeper experiments, injecting relatively close to the water table was found to result in significant changes in CO<sub>2</sub> saturation levels over short vertical distances. The change in the noble gas ratios suggests that between 0.156 kg and 0.529 kg (0.9% to 3.1%) of the injected CO<sub>2</sub> was degassed immediately after the injection period, prior to transport by the natural hydraulic gradient. Even with such a minor amount of degassing, the noble gas tracers were strongly depleted, especially He due to its low solubility (-85.0% to -80.4% for He and -34.2% to -13.9% for Kr under closed or open system conditions, respectively).

This study confirms the ability of these inert tracers to track even small amounts of CO<sub>2</sub> leakage as well as associated physiochemical processes during CO<sub>2</sub> migration, relying on the clear signals achieved by artificial enhancement. For an optimal monitoring efficiency, the combination of less soluble tracers such as SF<sub>6</sub> or He with relatively soluble tracers is recommended. Instead of artificial tracers, naturally occurring tracers could also be applied to achieve similar goals, however concentration changes during solubility-controlled processes must be consistent with analytical detection limits and experimental errors. Finally, the presented results show how, even amongst noble gas tracers, site specific conditions may influence the best choice of monitoring parameters for fast and efficient leakage detection.

## Acknowledgements

This research was supported by a Korea Environmental Industry & Technology Institute (KEITI) grant entitled "R&D Project on Environmental Management of Geologic CO<sub>2</sub> Storage" (Project Number: 2018001810002), by a Korea Polar Research Institute grant (PE19060) and by a National Research Foundation of Korea (NRF) grant funded by the Korean government (MSIT) (No. 0409-20190119). SEB acknowledges funding from the European Union's Horizon 2020 project ENOS ("Enabling Onshore CO<sub>2</sub> Storage in Europe" - Grant agreement 653718). We thank all the members of the K-COSEM team and, appreciate Intae Kim and Minjung Kim for their efforts and support on noble gas analysis. Finally, the authors would like to thank two anonymous reviewers for their detailed comments and observations which greatly improved the present paper.

$K_A, K_B$  = Henry's constant for A and B

$r_A, r_B$  = groundwater phase activity coefficients for A and B

$\phi_A, \phi_B$  = gas phase fugacity coefficients for A and B.

In an open system, there is a continuous loss of CO<sub>2</sub> bubbles until the end of the phase-partitioning process. The noble gas composition of the dissolved plume is gradually enriched with heavier elements with continuous degassing (Holland and Gilfillan, 2013; Zhou et al., 2005). The noble gas composition of the CO<sub>2</sub> plume, in this case, is a function of the remaining mass of elements. The Rayleigh equation can be used to describe such a system:

$$\left(\frac{A}{B}\right)_{(l)} = \left(\frac{A}{B}\right)_0 f^{\alpha-1}$$

$\left(\frac{A}{B}\right)_0$  = The composition of A and B in the initial injected plume  
 $f$  = Fraction of elements remaining in the dissolved plume  
 $\alpha$  = partitioning coefficient for gas/liquid system

## Appendix B. Iterative calculation of CO<sub>2</sub> budget

The degassed mass can be constrained iteratively and inversely using different noble gases (Ballentine et al., 2002; Holland and Gilfillan, 2013). This model assumes the progressive loss of small volumes of gas bubbles ( $V_g/V_i^0$ ) from the remaining CO<sub>2</sub> rich plume. The iteration steps in the model involve repeatedly reducing the remaining mass until the result fits with the observed noble gas data. The total degassed volume can be obtained by summing gas volumes in the final stage (Zhou et al., 2005). Two noble gases were used to determine the degassed mass such that:

$$m_{NG1(l)}^i = m_{NG1(l)}^{i-1} - m_{NG1(g)}^{i-1}$$

$$m_{NG2(l)}^i = m_{NG2(l)}^{i-1} - m_{NG2(g)}^{i-1}$$

where,

$i$  = Iteration step

$m_{(l)}^{i-1}$  = mass in dissolved phase before  $i - 1^{th}$  degassing loss (g)

$m_{(l)}^i$  = mass in dissolved phase after  $i - 1^{th}$  degassing loss (g)

$m_{(g)}^{i-1}$  = degassed mass during  $i - 1^{th}$  degassing process (g)

and degassed mass was determined from the degassed volume, such that:

$$m_{(g)}^{i-1} = C(V_g) \times p^{i-1}$$

$$C = M/V_m$$

$$p^{i-1} = \gamma K x^{i-1} / \phi$$

$$x^{i-1} = 18 [NG]^{i-1} (\rho_{(l)} V_{(l)})^{-1}$$

where,

$V_{(g)}$  = degassed volume during  $i - 1^{th}$  degassing process (cm<sup>3</sup>)

$C$  = conversion factor from volume to mass

$M$  = molar mass (g/mol)

$V_m$  = molar volume at ambient temperature and pressure (cm<sup>3</sup>/mol)

$p^{i-1}$  = partial pressure of removed noble gas during  $i - 1^{th}$  degassing process

$K$  = Henry's constant in units of pressure (atm)

$\gamma$  = liquid phase activity coefficient

$\phi$  = gas phase fugacity coefficient

$x^{i-1}$  = molar fraction of noble gas in dissolved phase at  $i - 1^{th}$  degassing moment (mol<sub>NG</sub>/mol<sub>(l)</sub>)

$[NG]^{i-1}$  = number of moles in dissolved phase at  $i - 1^{th}$  degassing moment (mol)

$\rho_{(l)}$  = density of dissolved phase (g/cm<sup>3</sup>)

$V_{(l)}$  = volume of dissolved phase (cm<sup>3</sup>)

For a closed system, a one-step degassing process was assumed where  $V_{(g)}$  was repeatedly adjusted to obtain the noble gas ratio of the monitoring data,  $\frac{m_{NG1(l)}^i}{m_{NG2(l)}^i}$ . For an open system, an iterative model was used with a fixed  $V_{(g)}$  value which should be small enough to finally achieve convergence with the measured noble gas composition. The noble gas concentration in the groundwater was gradually decreased in iterative steps. In the final stage ( $i = n$ ),  $\frac{m_{NG1(l)}^i}{m_{NG2(l)}^i}$  was matched against the monitored composition, and then the total degassed volume was calculated by multiplication of  $V_{(g)}$  and the number of iteration steps in the open system model.

## Appendix C. Supplementary data

Supplementary material related to this article can be found, in the online version, at doi:<https://doi.org/10.1016/j.ijggc.2019.05.002>.

## References

- Aeschbach-Hertig, W., Solomon, D.K., 2013. Noble gas thermometry in groundwater hydrology. In: Burnard, P. (Ed.), The Noble Gases as Geochemical Tracers. Advances in Isotope Geochemistry. Springer, Berlin, Heidelberg, pp. 81–122. [https://doi.org/10.1007/978-3-642-28836-4\\_5](https://doi.org/10.1007/978-3-642-28836-4_5).
- Ballentine, C.J., Schoell, M., Coleman, D., Cain, B.A., 2001. 300-Myr-old magmatic CO<sub>2</sub> in

- natural gas reservoirs of the west Texas Permian basin. *Nature* 409 (6818), 327–331. <https://doi.org/10.1038/35053046>.
- Ballentine, C.J., Burgess, R., Marty, B., 2002. Tracing fluid origin, transport and interaction in the crust. In: Porcelli, D., Ballentine, C.J., Wieler, R. (Eds.), *Reviews in Mineralogy & Geochemistry Volume 47, Noble Gases in Geochemistry and Cosmochemistry*, pp. 539–614.
- Bayer, R., Schlosser, P., Bönisch, G., Rupp, H., Zaucker, F., Zimmek, G., 1989. Performance and blank components of a mass spectrometric system for routine measurement of helium isotopes and tritium by the  $^3\text{He}$  ingrowth method. *Sitzungsberichte der Heidelberger Akademie der Wissenschaften, Mathematisch-naturwissenschaftliche Klasse. Jahrgang 5*, 241–279. <https://doi.org/10.1007/978-3-642-48373-8>.
- Beaubien, S.E., Bigi, S., Lombardi, S., Sacco, P., Tartarello, M.C., 2014. Groundwater changes caused by flow through naturally occurring gas ( $\pm$  water) leakage points. *4th EAGE CO<sub>2</sub> Geological Storage Workshop*.
- Boyd, A.D., 2016. Risk perceptions of an alleged CO<sub>2</sub> leak at a carbon sequestration site. *Int. J. Greenh. Gas Control* 50, 231–239. <https://doi.org/10.1016/j.ijggc.2016.03.025>.
- Cahill, A.G., Marker, P., Jakobsen, R., 2014. Hydrogeochemical and mineralogical effects of sustained CO<sub>2</sub> contamination in a shallow sandy aquifer: a field-scale controlled release experiment. *Water Resour. Res.* 50 (2), 1735–1755. <https://doi.org/10.1002/2013WR014294>.
- Carrigan, C.R., Heinle, R.A., Hudson, G.B., Nitaio, J.J., Zucca, J.J., 1996. Trace gas emissions on geological faults as indicators of underground nuclear testing. *Nature* 382 (6591), 528–531.
- Celia, M.A., 2017. Geological storage of captured carbon dioxide as a large-scale carbon mitigation option. *Water Resour. Res.* 53, 3527–3533. <https://doi.org/10.1002/2017WR020841>.
- Darrah, T.H., Vengosh, A., Jackson, R.B., Warner, N.R., Poreda, R.J., 2014. Noble gases identify the mechanisms of fugitive gas contamination in drinking-water wells overlying the Marcellus and Barnett Shales. *Proc. Natl. Acad. Sci. U. S. A.* 111 (39), 14076–14081. <https://doi.org/10.1073/pnas.1322107111>.
- Dickson, A.G., Sabine, C.L., Christian, J.R., 2007. Guide to Best Practices for Ocean CO<sub>2</sub> Measurements. pp. 191. (IPCES Special Publication 3). North Pacific Marine Science Organization, Sidney, British Columbia. <http://hdl.handle.net/11329/249>.
- Gilfillan, S.M.V., Ballentine, C.J., Holland, G., Blagburn, D., Sherwood Lollar, B., Scott, S., Schoell, M., Cassidy, M., 2008. The noble gas geochemistry of natural CO<sub>2</sub> gas reservoirs from the Colorado Plateau and Rocky Mountain provinces, USA. *Geochim. Cosmochim. Acta* 72, 1174–1198. <https://doi.org/10.1016/j.gca.2007.10.009>.
- Gilfillan, S.M.V., Wilkinson, M., Haszeldine, R.S., Shipton, Z.K., Nelson, S.T., Poreda, R.J., 2011. He and Ne as tracers of natural CO<sub>2</sub> migration up a fault from a deep reservoir. *Int. J. Greenh. Gas Control* 5 (6), 1507–1516. <https://doi.org/10.1016/j.ijggc.2011.08.008>.
- Gilfillan, S.M.V., Sherk, G.W., Poreda, R.J., Haszeldine, R.S., 2017. Using noble gas fingerprints at the Kerr farm to assess CO<sub>2</sub> leakage allegations linked to the Weyburn-Midale CO<sub>2</sub> monitoring and storage project. *Int. J. Greenh. Gas Control* 63, 215–225. <https://doi.org/10.1016/j.ijggc.2017.05.015>.
- Györe, D., Stuart, F.M., Gilfillan, S.M.V., Waldron, S., 2015. Tracing injected CO<sub>2</sub> in the cranfield enhanced oil recovery field (MS, USA) using He, Ne and Ar isotopes. *Int. J. Greenh. Gas Control* 42, 554–561. <https://doi.org/10.1016/j.ijggc.2015.09.009>.
- Györe, D., Gilfillan, S.M.V., Stuart, F.M., 2017. Tracking the interaction between injected CO<sub>2</sub> and reservoir fluids using noble gas isotopes in an analogue of large-scale carbon capture and storage. *Appl. Geochem.* 78, 116–128. <https://doi.org/10.1016/j.apgeochem.2016.12.012>.
- Györe, D., McKavney, R., Gilfillan, S.M.V., Stuart, F.M., 2018. Fingerprinting coal-derived gases from the UK. *Chem. Geol.* 480, 75–85. <https://doi.org/10.1016/j.chemgeo.2017.09.016>.
- Hebig, K.H., Zeifelder, S., Ito, N., Machida, I., Marui, A., Scheytt, T.J., 2015. Study of the effects of the chaser in push-pull tracer tests by using temporal moment analysis. *Geothermics* 54, 43–53. <https://doi.org/10.1016/j.geothermics.2014.11.004>.
- Holland, G., Gilfillan, S., 2013. Application of noble gases to the viability of CO<sub>2</sub> storage. In: Burnard, P. (Ed.), *The Noble Gases as Geochemical Tracers. Advances in Isotope Geochemistry*. Springer, Berlin, Heidelberg, pp. 177–223. [https://doi.org/10.1007/978-3-642-28836-4\\_8](https://doi.org/10.1007/978-3-642-28836-4_8).
- Humez, P., Négrel, P., Lagneau, V., Lions, J., Kloppmann, W., Gal, F., Millot, R., Guerrot, C., Flehoc, C., Widory, D., Girard, J.-F., 2014. CO<sub>2</sub>-water-mineral reactions during CO<sub>2</sub> leakage: geochemical and isotopic monitoring of a CO<sub>2</sub> injection field test. *Chem. Geol.* 368, 11–30. <https://doi.org/10.1016/j.chemgeo.2014.01.001>.
- IPCC, 2005. IPCC special report on carbon dioxide capture and storage. In: Metz, B., Davidson, O., de Coninck, H.C., Loos, M., Meyer, L.A. (Eds.), *Prepared by Working Group III of the Intergovernmental Panel on Climate Change*. Cambridge University Press, Cambridge, United Kingdom/New York, NY, USA pp. 208–210.
- Ju, Y., Kaown, D., Lee, K.-K., 2018. A three-pronged approach for identifying source and extent of nitrate contamination in groundwater. *J. Soil Water Conserv.* 73 (5), 493–503. <https://doi.org/10.2489/jswc.73.5.493>.
- Keating, E.H., Fessenden, J., Kanjorski, N., Koning, D.J., Pawar, R., 2010. The impact of CO<sub>2</sub> on shallow groundwater chemistry: observations at a natural analog site and implications for carbon sequestration. *Environ Earth Sci* 60, 521–536. <https://doi.org/10.1007/s12665-009-0192-4>.
- Kharaka, Y.K., Cole, D.R., Hovorka, S.D., Gunter, W.D., Knauss, K.G., Freifeld, B.M., 2006. Gas-water-rock interactions in Frio formation following CO<sub>2</sub> injection: implications for the storage of greenhouse gases in sedimentary basins. *Geology* 34 (7), 577–580. <https://doi.org/10.1130/G22357.1>.
- Kilgallon, R., Gilfillan, S.M.V., Edlmann, K., McDermott, C.I., Naylor, M., Haszeldine, R.S., 2018. Experimental determination of noble gases and SF<sub>6</sub> as tracers of CO<sub>2</sub> flow through porous sandstone. *Chem. Geol.* 480, 93–104. <https://doi.org/10.1016/j.chemgeo.2017.09.022>.
- Kim, H.H., 2017. Application of Push-Drift-Pull Tracer Tests at a CO<sub>2</sub> Storage Environmental Test Site and Identification of Factors Affecting Breakthrough Curves (M.S. Dissertation, Seoul National University). <http://hdl.handle.net/10371/131434>.
- Kim, I., Hahn, D., Rhee, T.S., Kim, T.W., Kim, C.-S., Lee, S., 2016. The distribution of glacial meltwater in the Amundsen Sea, Antarctica, revealed by dissolved helium and neon. *J. Geophys. Res.: Oceans* 121 (3), 1654–1666. <https://doi.org/10.1002/2015JC011211>.
- Kim, H.-H., Lee, S.-S., Ha, S.-W., Lee, K.-K., 2018. Application of single-well push-drift-pull tests using dual tracers (SF<sub>6</sub> and salt) for designing CO<sub>2</sub> leakage monitoring network at the environmental impact test site in Korea. *Geosci. J.* 22 (6), 1041–1052. <https://doi.org/10.1007/s12303-018-0045-9>.
- Kipfer, R., Aeschbach-Hertig, W., Peeters, F., Stute, M., 2002. Noble gases in lakes and ground waters. In: Porcelli, D., Ballentine, C.J., Wieler, R. (Eds.), *Noble Gases in Geochemistry and Cosmochemistry*. Rev. Mineral. Geochem. 47, pp. 615–700. <https://doi.org/10.2138/rmg.2002.47.14>.
- KMOE, 2017. Hydraulic Characterization and Shallow-Depth Ground Water Monitoring for Evaluation of Environmental Impacts Caused by CO<sub>2</sub> Storage and Leakage, Annual Report (Year III, Phase I), Prepared by Korea Ministry of Environment. pp. 432–433 (in Korean).
- LaForce, T., Ennis-King, J., Boreham, C., Paterson, L., 2014. Residual CO<sub>2</sub> saturation estimate using noble gas tracers in a single-well field test: the CO<sub>2</sub>CRC otway project. *Int. J. Greenh. Gas Control* 26, 9–21. <https://doi.org/10.1016/j.ijggc.2014.04.009>.
- Laforce, S., Moreira, A., Agrinier, P., Bonneville, A., Schneider, H., Catalette, H., 2009. Noble gases as tools for subsurface monitoring of CO<sub>2</sub> leakage. *Energy Procedia* 1 (1), 2185–2192. <https://doi.org/10.1016/j.egypro.2009.01.284>.
- Lee, K.-K., Lee, S.H., Yun, S.-T., Jeon, S.-W., 2016. Shallow groundwater system monitoring on controlled CO<sub>2</sub> release sites: a review on field experimental methods and efforts for CO<sub>2</sub> leakage detection. *Geosci. J.* 20 (4), 569–583. <https://doi.org/10.1007/s12303-015-0060-z>.
- Lee, S.H., Kim, S.-O., Choi, B.-Y., Do, H.-K., Yun, S.-T., Jun, S.-C., 2017a. Hydrogeochemical modeling on water-rock-CO<sub>2</sub> interactions within a CO<sub>2</sub>-injected shallow aquifer. *J. Geol. Soc. Korea* 53 (5), 657–673. <https://doi.org/10.14770/jgsk.2017.53.5.657>.
- Lee, S.S., Kim, H.H., Joun, W.T., Lee, K.K., 2017b. Design and construction of groundwater monitoring network at shallow-depth CO<sub>2</sub> injection and Leak Test Site, Korea. *Energy Procedia* 114, 3060–3069. <https://doi.org/10.1016/j.egypro.2017.03.1434>.
- Lott, D.E., 2001. Improvements in noble gas separation methodology: a nude cryogenic trap. *Geochim. Geophys. Geosyst.* 2 (12), 1–13. <https://doi.org/10.1029/2001GC000202>.
- Lott, D.E., Jenkins, W.J., 1998. Advances in analysis and shipboard processing of tritium and helium samples. *Int. WOCE Newsletter*, 30, 27–30.
- Lu, J., Cook, P.J., Hosseini, S.A., Yang, C., Romanak, K.D., Zhang, T., Freifeld, B.M., Smyth, R.C., Zeng, H., Hovorka, S.D., 2012. Complex fluid flow revealed by monitoring CO<sub>2</sub> injection in a fluvial formation. *J. Geophys. Res. Solid Earth* 117 (B3), 1–13. <https://doi.org/10.1029/2011JB008939>.
- Ma, L., Castro, M.C., Hall, C.M., 2009. Atmospheric noble gas signatures in deep Michigan Basin brines as indicators of a past thermal event. *Earth Planet Sci. Lett.* 277 (1–2), 137–147. <https://doi.org/10.1016/j.epsl.2008.10.015>.
- Macpherson, G.L., Roberts, J.A., Blair, J.M., Townsend, M.A., Fowle, D.A., Beisner, K.R., 2008. Increasing shallow groundwater CO<sub>2</sub> and limestone weathering, Konza Prairie, USA. *Geochim. Cosmochim. Acta* 72 (23), 5581–5599. <https://doi.org/10.1016/j.gca.2008.09.004>.
- Manning, A.H., Solomon, D.K., Thiros, S.A., 2005. 3H/3He age data in assessing the susceptibility of wells to contamination. *Groundwater* 43 (3), 353–367. <https://doi.org/10.1111/j.1745-6584.2005.0028.x>.
- Nimz, G.J., Hudson, G.B., 2005. The use of noble gas isotopes for monitoring leakage of geologically stored CO<sub>2</sub>. In: In: Thomas, D.C., Benson, S.M. (Eds.), *Carbon Dioxide Capture for Storage in Deep Geologic Formations*, vol. 2. Elsevier Press, Amsterdam, pp. 1113–1128.
- Ozima, M., Podosek, F.A., 2002. *Noble Gas Geochemistry*, 2nd ed. Cambridge University Press, Cambridge, pp. 367–367.
- Park, G.-H., Lee, K., Tishchenko, P., 2008. Sudden, considerable reduction in recent uptake of anthropogenic CO<sub>2</sub> by the East/Japan Sea. *Geophys. Res. Lett.* 35 (23), L23611. <https://doi.org/10.1029/2008GL036118>.
- Parkhurst, D.L., Appelo, C.A.J., 2013. Description of input and examples for PHREEQC version 3—A computer program for speciation, batch-reaction, one-dimensional transport, and inverse geochemical calculations. U.S. Geological Survey Techniques and Methods, Book 6, A43, 497. available only at <http://pubs.usgs.gov/tm/06/a43>.
- Peter, A., Lamert, H., Beyer, M., Hornbruch, G., Heinrich, B., Schulz, A., Geistlinger, H., Schreiber, B., Dietrich, P., Werban, U., Vogt, C., Richnow, H.-H., Großmann, J., Dahmke, A., 2012. Investigation of the geochemical impact of CO<sub>2</sub> on shallow groundwater: design and implementation of a CO<sub>2</sub> injection test in northeast Germany. *Environ. Earth Sci.* 67 (2), 335–349. <https://doi.org/10.1007/s12665-012-1700-5>.
- Risk, D., Lavoie, M., Nickerson, N., 2015. Using the Kerr investigations at Weyburn to screen geochemical tracers for near-surface detection and attribution of leakage at CCS/EOR sites. *Int. J. Greenh. Gas Control* 35, 13–17. <https://doi.org/10.1016/j.ijggc.2015.01.019>.
- Sakaki, T., Plampin, M.R., Pawar, R., Komatsu, M., Illangasekare, T.H., 2013. What controls carbon dioxide gas phase evolution in the subsurface? Experimental observations in a 4.5 m-long column under different heterogeneity conditions. *Int. J. Greenh. Gas Control* 17, 66–77. <https://doi.org/10.1016/j.ijggc.2013.03.025>.
- Sander, R., 2017. Henry's law constants. In: Linstrom, P.J., Mallard, W.G. (Eds.), NIST Chemistry WebBook, NIST Standard Reference Database Number 69. National

- Institute of Standards and Technology, Gaithersburg MD, pp. 20899. <https://doi.org/10.18434/T4D303>.
- Sanford, W.E., Shropshire, R.G., Solomon, D.K., 1996. Dissolved gas tracers in groundwater: simplified injection, sampling, and analysis. *Water Resour. Res.* 32 (6), 1635–1642. <https://doi.org/10.1029/96WR00599>.
- Sathaye, K.J., Hesse, M.A., Cassidy, M., Stockli, D.F., 2014. Constraints on the magnitude and rate of CO<sub>2</sub> dissolution at Bravo Dome natural gas field. *PNAS* 111 (43), 15332–15337. <https://doi.org/10.1073/pnas.1406076111>.
- Schulz, A., Vogt, C., Lamert, H., Peter, A., Heinrich, B., Dahmke, A., Richnow, H.-H., 2012. Monitoring of a simulated CO<sub>2</sub> leakage in a shallow aquifer using stable carbon isotopes. *Environ. Sci. Technol.* 46 (20), 11243–11250. <https://doi.org/10.1021/es3026837>.
- Sherwood Lollar, B., Ballentine, C.J., Onions, R.K., 1997. The fate of mantle-derived carbon in a continental sedimentary basin: integration of C/He relationships and stable isotope signatures. *Geochim. Cosmochim. Acta* 61 (11), 2295–2307. [https://doi.org/10.1016/S0016-7037\(97\)00083-5](https://doi.org/10.1016/S0016-7037(97)00083-5).
- Shevalier, M., Nightingale, M., Mayer, B., Hutcheon, I., Durocher, K., Perkins, E., 2013. Brine geochemistry changes induced by CO<sub>2</sub> injection observed over a 10 year period in the Weyburn oil field. *Int. J. Greenh. Gas Technol.* 16S, S160–S176. <https://doi.org/10.1016/j.ijggc.2013.02.017>.
- Solomon, D.K., Genereux, D.P., Plummer, L.N., Busenberg, E., 2010. Testing mixing models of old and young groundwater in a tropical lowland rain forest with environmental tracers. *Water Resour. Res.* 46 (4), W04518. <https://doi.org/10.1029/2009WR008341>.
- Solomon, D.K., Gilmore, T.E., Solder, J.E., Kimball, B., Genereux, D.P., 2015. Evaluating an unconfined aquifer by analysis of age-dating tracers in stream water. *Water Resour. Res.* 51 (11), 8883–8899. <https://doi.org/10.1002/2015WR017602>.
- Stalker, L., Boreham, C., Underschultz, J., Freifeld, B., Perkins, E., Schacht, U., Sharma, S., 2009. Geochemical monitoring at the CO<sub>2</sub>CRC otway project: tracer injection and reservoir fluid acquisition. *Energy Procedia* 1 (1), 2119–2125. <https://doi.org/10.1016/j.egypro.2009.01.276>.
- Stalker, L., Boreham, C., Underschultz, J., Freifeld, B., Perkins, E., Schacht, U., Sharma, S., 2015. Application of tracers to measure, monitor and verify breakthrough of sequestered CO<sub>2</sub> at the CO<sub>2</sub>CRC Otway project, Victoria, Australia. *Chem. Geol.* 399, 2–19. <https://doi.org/10.1016/j.chemgeo.2014.12.006>.
- Stanley, R.H., Jenkins, W.J., 2013. Noble gases in seawater as tracers for physical and biogeochemical ocean processes. In: Burnard, P. (Ed.), *The Noble Gases as Geochemical Tracers. Advances in Isotope Geochemistry*. Springer, Berlin, Heidelberg, pp. 55–79. [https://doi.org/10.1007/978-3-642-28836-4\\_4](https://doi.org/10.1007/978-3-642-28836-4_4).
- Stanley, R.H., Jenkins, W.J., Lott, D.E., Doney, S.C., 2009. Noble gas constraints on air-sea gas exchange and bubble fluxes. *J. Geophys. Res.: Oceans* 114 (C11), C11020. <https://doi.org/10.1029/2009JC005396>.
- Susanto, V., Sasaki, K., Sugai, Y., Kawasaki, W., 2016. Field test study on leakage monitoring at a geological CO<sub>2</sub> storage site using hydrogen as a tracer. *Int. J. Greenh. Gas Control* 50, 37–48. <https://doi.org/10.1016/j.ijggc.2016.04.001>.
- Trautz, R.C., Pugh, J.D., Varadharajan, C., Zheng, L., Bianchi, M., Nico, P.S., Spycher, N.F., Newell, D.L., Esposito, R.A., Wu, Y., Dafflon, B., Hubbard, S.S., Birkholzer, J.T., 2012. Effect of dissolved CO<sub>2</sub> on a shallow groundwater system: a controlled release field experiment. *Environ. Sci. Technol.* 47 (1), 298–305. <https://doi.org/10.1021/es301280t>.
- Vesper, D.J., Edenborn, H.M., 2012. Determination of free CO<sub>2</sub> in emergent groundwaters using a commercial beverage carbonation meter. *J. Hydrol.* 438–439, 148–155. <https://doi.org/10.1016/j.jhydrol.2012.03.015>.
- Wilkinson, M., Gilfillan, S.M.V., Haszeldine, R.S., Ballentine, C.J., 2010. Plumbing the depths: testing natural tracers of subsurface CO<sub>2</sub> origin and migration, Utah. In: In: Grobe, M., Pashin, J.C., Dodge, R.L. (Eds.), *Carbon Dioxide Sequestration in Geological Media – State of the Science 59*. American Association of Petroleum Geologists Studies, pp. 619–634. <https://doi.org/10.1306/13171266St591353>.
- Yang, C., Hovorka, S.D., Young, M.H., Trevino, R., 2014. Geochemical sensitivity to CO<sub>2</sub> leakage: detection in potable aquifers at carbon sequestration sites. *Greenhouse Gases Sci. Technol.* 4 (3), 384–399. <https://doi.org/10.1002/ghg.1406>.
- Zhang, Y., Freifeld, B., Finsterle, S., Leahy, M., Ennis-King, J., Paterson, L., Dance, T., 2011. Single-well experimental design for studying residual trapping of supercritical carbon dioxide. *Int. J. Greenh. Gas Control* 5 (1), 88–98. <https://doi.org/10.1016/j.ijggc.2010.06.011>.
- Zhou, Z., Ballentine, C.J., Kipfer, R., Schoell, M., Thibodeaux, S., 2005. Noble gas tracing of groundwater/coalbed methane interaction in the San Juan Basin. USA. *Geochim. Cosmochim. Acta* 69 (23), 5413–5428. <https://doi.org/10.1016/j.gca.2005.06.027>.